Photoactivated Adenylate Cyclases: Photochemistry and Signaling Transduction

A Dissertation Presented

by

Samruddhi Sanjay Jewlikar

to

The Graduate School

in Partial Fulfillment of the

Requirements

For the degree of

Doctor of Philosophy

in

Biochemistry and Structural Biology

Stony Brook University

January 2025

Stony Brook University

The Graduate School

Samruddhi Sanjay Jewlikar

We, the dissertation committee for the above candidate for the

Doctor of Philosophy degree, hereby recommend

Acceptance of this dissertation.

Peter J. Tonge – Dissertation Supervisor
Distinguished Professor of Chemistry, Stony Brook University

Christopher Brownlee – Chairperson of Defense
Assistant Professor of Pharmacological Sciences, Stony Brook University

Michael Airola – Third Member
Associate Professor of Biochemistry and Cell Biology, Stony Brook University

Erwin London- Fourth Member
Distinguished Professor of Biochemistry and Cell Biology, Stony Brook University

This dissertation is accepted by the Graduate School

Celia Marshik

Dean of the Graduate School

Abstract of the Dissertation

Photoactivated Adenylate Cyclases: Photochemistry and Signaling Transduction

by

Samruddhi Sanjay Jewlikar

Doctor of Philosophy

in

Biochemistry and Structural Biology

Stony Brook University

2025

OaPAC, the photoactivated adenylate cyclase from *Oscillatoria acuminata*, is comprised of a Blue Light using FAD (BLUF) domain fused to an adenylate cyclase (AC) domain. Since both the BLUF and AC domains are part of the same protein, OaPAC is a model for understanding how the ultrafast modulation of the chromophore binding pocket caused by photoexcitation results in the activation of the output domain on the μs-s timescale. There is significant interest in understanding how ultrafast photoexcitation controls biological functions, such as phototaxis, gene expression, and virulence. This information can drive the development of novel optogenetic tools. In this dissertation, we first employed ultrafast vibrational spectroscopy to characterize the intermediate steps that lead to formation of the light state. Then, we probed the role of the conserved tyrosine (Tyr 6) in the forward reaction by replacing this residue with fluorotyrosine analogues. Tyr 6 plays a crucial role in the photochemistry, and the use of fluorotyrosine analogues allowed us to assess the effect of modulating the pKa and/or reduction potential of Tyr 6 on the

activation of the adenylate cyclase domain which catalyzes the conversion of ATP to cAMP and PPi. Time-resolved vibrational spectroscopy reveals that the photoactivation of OaPAC involves radical intermediates and that an increase in acidity of Tyr 6 halts the photocycle, preventing light-state formation. In agreement with this observation, we demonstrate that an increase in acidity of Tyr 6 also prevents activation of the adenylate cyclase domain.

OaPAC is a model system comprising of output domain covalently linked to sensory BLUF photoreceptor domain. Hence, we expanded our studies to elucidate the signaling transduction mechanism in OaPAC. We employed unnatural amino acid mutagenesis to identify specific sites in the protein that are involved in transducing the signal from the FAD binding site to the ATP binding site. To provide insight into site-specific structural dynamics, we replaced W90 which is close to the chromophore pocket, F103 which interacts with W90 across the dimer interface, and F180 in the central core of the AC domain, with the infrared probe azido-Phe (AzPhe). Using ultrafast IR, we show that AzPhe at position 90 responds on multiple timescales following photoexcitation. In contrast, the light minus dark IR spectrum of AzPhe103 shows only a minor perturbation in environment between the dark and light states, while replacement of F180 with AzPhe resulted in a protein with no catalytic activity. We also replaced Y125, which hydrogen bonds with N256 across the dimer interface, with fluoro-Tyr residues. All the fluoro-Tyr substituted proteins retained the light induced red shift in the flavin absorption spectrum, however only the 3-FY125 OaPaC retained photoinduced catalytic activity. The loss of activity in 3,5-F_2Y125 and 2,3,5-F_3Y125 OaPaC, which potentially increase the acidity of the Y125 phenol by more than a 1000-fold, suggests that deprotonation of Y125 disrupts the signal transduction pathway from the BLUF to the AC domain.

Dedication page

To my parents, Aparna and Sanjay who gave me the values that I treasure immensely, who always believed in me and gave me the freedom to dream big, who always gave me their unconditional love and support to create a life for myself. To my younger brother, Samarth for his unconditional love and care. To my husband, Siddhesh and my in-laws Rohini and Sandeep for their love, care and unwavering support and encouragement.

To my mentors in professional and personal life, who have inspired me and taught me wisdom. To my friends who have been a great support system, who made my life in the US easier and with whom I have made precious memories.

To all the life experiences that have been my greatest teachers! My heart is filled with immense gratitude!

Table of Contents

List of Figures/Tables/Illustrations

Chapter 1

Chapter 2:

Chapter 3:

List of tables

Chapter 2

Chapter 3

List of Abbreviations

3-FY	3-Fluorotyrosine
2,3-F_2Y	2,3-difluorotyrosine
3,5-F_2Y	3,5-difluorotyrosine
2,3,5-F_3Y	2,3,5-trifluorotyrosine
AC	Adenylate cyclase
Amp	Ampicillin
ATP	Adenosine triphosphate
AppA	Activation of photopigment and puc
$AppA_{BLUF}$	blue light using FAD domain of AppA
$AppA_{FULL}$	AppA full length
Arg (R)	Arginine
Asn (N)	Asparagine
Asp (D)	Aspartic acid
BlsA	Blue light sensing protein A
BLUF	Blue light using FAD
cAMP	Cyclic Adenosine Monophosphate
C	Celsius
cm^{-1}	Wavenumber
ES	Excited state
ET	Electron transfer
FAD	Flavin adenine dinucleotide
FMN	Flavin mononucleotide
fs	femtosecond
FTIR	Fourier transform infrared
FY	Fluorotyrosine
Gln (Q)	Glutamine
Glu (E)	Glutamic acid
GS	Ground state
H-bond	Hydrogen bond
IPTG	Isopropyl-beta-D-thiogalactopyranoside
IR	Infrared
L	Liter
LB	Luria-Bertani broth
LOV	Light Oxygen Voltage
Met (M)	Methionine
$MgCl_2$	Magnesium Chloride
ms	Millisecond
min	Minute
mL	Milliliter
mM (mmol)	Millimolar
nm	Nanometer
ns	Nanosecond
OD600	Optical density at 600 nm

OaPAC	Photoactivated adenylyl cyclase (AC) from Oscillatoria Acuminata
PAC	Photoactivated adenylyl cyclase
PAGE	Polyacrylamide gel electrophoresis
PCET	Proton- coupled electron transfer
PDB	Protein database
Phe (F)	Phenylalanine
PixD	Positive phototaxis protein D
PixE	Positive phototaxis protein E
PMSF	Phenylmethanesulfonylfluoride
ps	picosecond
PP_i	Pyrophosphate
PT	Proton transfer
RPM	Revolutions per minute
QY	Quantum yield
TPL	Tyrosine Phenol Lyase
TRIR	Time-resolved infrared
TRMPS	Time-resolved multiple probe spectroscopy
Trp (W)	Tryptophan
Tyr (Y)	Tyrosine
UV	Ultraviolet
Vis	Visible
WT	Wild-type

Acknowledgements

First and foremost, I want to start by acknowledging my advisor Prof. Peter J. Tonge. It all began when I had several inspiring and engaging scientific conversations with Prof. Tonge during my rotation. I want to thank Prof. Tonge for always being there whenever I needed help. Thank you for always being welcoming towards the questions and curiosities that I had. I am grateful for all the wisdom, guidance, support, care, kindness and patience that you have provided over the years. Thank you for giving me the opportunity to be a part of your research group. I am grateful for being a part of the Tonge lab group where I met many amazing scientists and where I even gained friends for life.

Next, I want to thank Dr. Jinnette Tolentino Collado for being my mentor in my PhD journey. Thanks Jinnette, for your guidance, mentorship, kindness and wonderful scientific discussions. It will always be in my memory how we worked together until late at night to purify the proteins and perform the enzyme assays all on the same day.

I would like to thank Prof. Steve Meech for making the collaboration between RAL and our research group possible.

I am grateful to my committee members, Prof. Erwin London, Dr. Christopher Brownlee and Dr. Michael Airola for their constructive guidance, support, understanding and for making my defense day possible.

I am very grateful for all the help I got from the Chemistry department, especially from Katherine Hughes. Thank you, Katherine, for always being available for us.

Publications

Jewlikar, S., Tolentino Collado, J., Ali, M., Sabbah, A., He, Y., Iuliano, J.N., Hall, C.R., Adamczyk, A., Greetham, G.M., Lukacs, A., Meech, S.R. and Tonge, P.J., Probing the signaling transduction mechanism of the blue light-activated adenylate cyclase OaPAC using unnatural amino acid mutagenesis. *[Manuscript accepted for publication in ACS Chemical Biology]*

Tolentino Collado, J., Iuliano, J.N., Pirisi, K., **Jewlikar, S.**, Adamczyk, K., Greetham, G.M., Towrie, M., Tame, J.R., Meech, S.R., Tonge, P.J. and Lukacs, A., 2022. Unraveling the Photoactivation Mechanism of a Light-Activated Adenylyl Cyclase Using Ultrafast Spectroscopy Coupled with Unnatural Amino Acid Mutagenesis. *ACS Chemical Biology*, 17(9), pp.2643-2654.

Chapter 1

Chapter 1: Introduction to BLUF Photoreceptors

The ability to sense and respond to environmental stimuli is a fundamental characteristic of living organisms. Light in the near-UV to near-infrared region of the electromagnetic spectrum is a vital environmental stimulus processed by diverse organisms across all kingdoms of life. Light acts as the primary energy source for photosynthesis, but its role extends to far beyond this fundamental process. It carries essential spatial and temporal information, providing organisms with crucial data and about their environment.[1]

To harness the informational content of incident light and regulate biological processes, nature has developed a wide array of sensory photoreceptor proteins. These specialized proteins enable organisms to detect light intensity, perceive different wavelengths and respond to changes in light conditions etc. Through these photoreceptors, organisms can fine-tune their physiological and behavioral responses to light, enhancing their survival and reproductive success in various environments.[1]

The photosensor or "input" module is responsible for light detection and contains an organic chromophore. When the chromophore absorbs light of the appropriate wavelength, it undergoes a conformational change, triggering the initial step of the signaling cascade. The effector or "output" module is responsible for initiating downstream biological responses. Once activated by the photosensor module, the effector module elicits various physiological changes within the cell.[1]

There are six well-characterized photoreceptor families found in nature to mediate light-induced signal transduction, namely the rhodopsins, phytochromes, xanthopsins, cryptochromes, phototropins, and BLUF proteins.[2] Amongst these families, cryptochromes,

phototropins and BLUF proteins can be clubbed together into a family of flavoproteins. Representative member of each of rhodopsins, phytochromes, xanthopsins and flavoproteins is shown in **Figure 1.1**. The family of flavoproteins contains receptors with light-oxygen-voltage (LOV) sensing domains; blue-light-utilizing flavin adenine dinucleotide (BLUF) domains; and cryptochromes.[3]

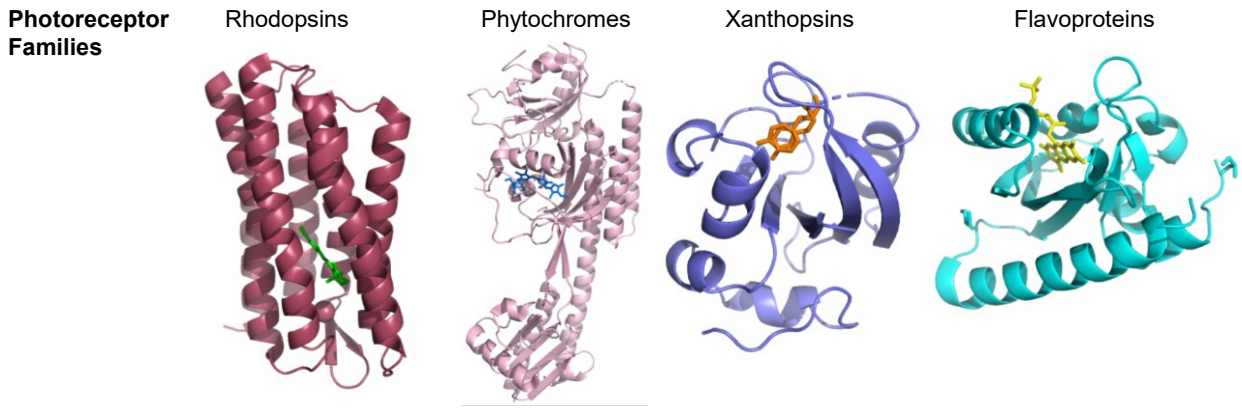

Figure 1.1. Photoreceptor families. Examples of photoreceptor families found in nature, with their respective chromophores and photochemistry. Figures made in PyMOL using PDB codes: 1H68, 6TL4, 2PYR, 2V1A respectively for representatives of rhodopsins, phytochromes, xanthopsins and flavoproteins family.[4,5,6,7]

These families convert light signal into biochemical signal using different mechanisms. The rhodopsins, phytochromes and xanthopsins catalyze cis to trans photoisomerization of retinal, phytochromobilin and p-coumaric acid chromophores respectively to activate the protein. However, flavoproteins have a different flavin-based photochemistry. The activation of flavoproteins does not require a large conformational change of the chromophore, and instead the protein must sense changes in the electronic structure of the flavin. Although some aspects of the photochemistry performed by this photoreceptor family has been delineated, for example electron and/or proton transfer in the case of the BLUF and

photolyase/cryptochromes, and cysteinyl adduct formation in the case of the LOV domain photoreceptors, the precise signaling mechanisms are still being elucidated.

My dissertation investigates the light- activated mechanism and signaling transduction of BLUF photoreceptor OaPAC by employing time-resolved infrared spectroscopy combined with incorporation of unnatural amino acids (UAAs). Chapter 1 discusses in detail the model system (proteins and chromophore), as well as the specific methods employed to monitor the primary events of the light-induced reaction and the signaling transductions upon photoexcitation. Chapter 2 and 3 goes into more detail on what we have accomplished in elucidating the photoactivation and signal transduction mechanism of the BLUF protein OaPAC and the use of azido-phenylalanine as a vibrational reporter to monitor time-dependent AzPhe response to structural dynamics or light-induced electron transfer reaction triggered by photoexcitation of the chromophore.

Flavin Chemistry and Photochemistry

Flavins are a class of compounds characterized by a 7,8-dimethylisoalloxazine heteroaromatic ring system. These molecules serve as essential cofactors in proteins and play pivotal roles in numerous cellular processes.[8] The structure of flavin derivatives is shown in **Figure 1.2A**. The remarkable chemical versatility of the flavin chromophore arises from its capacity to undergo various redox transformations through electron and proton transfer reactions. **Figure 1.2B** shows the oxidized (flavoquinone), one electron reduced (semiquinone), and two electrons reduced (hydroquinone) states of the isoalloxazine ring and their physiological ionic states. Flavoproteins have traditionally been recognized for their role in oxidation-reduction reactions in biological systems. However, three major classes of flavoproteins have now been identified as light-sensing proteins that regulate a wide range of biological processes across bacteria, plants, fungi, and animals.[9]

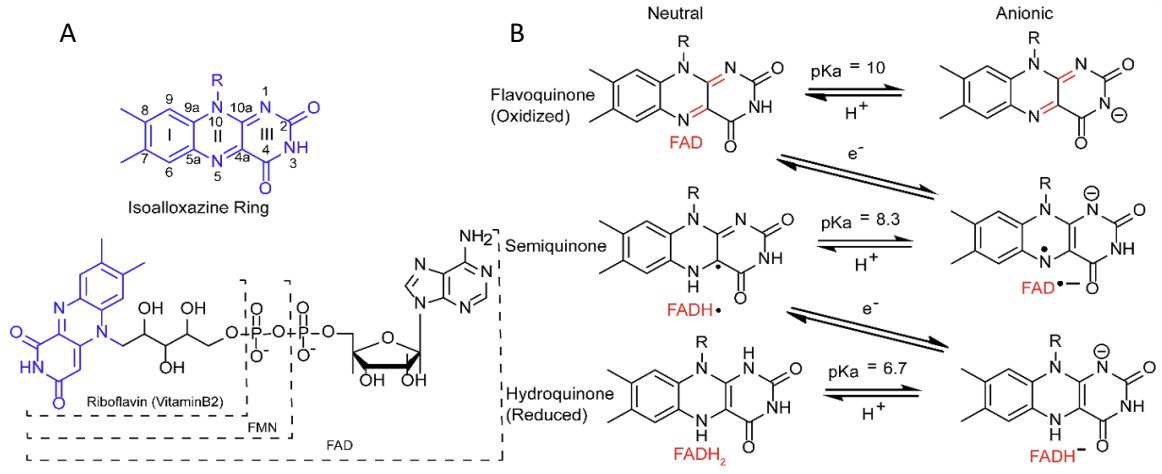

Figure 1.2. Structure of the flavin cofactor. (A) Forms of the flavin cofactor and numbering of the isoalloxazine ring. (B) Redox and ionic states of the isoalloxazine ring. Figure adapted from J. Li and T. Kitagawa.

The three major classes of flavin photosensors consist of light-oxygen-voltage (LOV) domains, blue-light-utilizing FAD (BLUF) proteins, and photolyases/cryptochromes (CRYs).[10] They noncovalently bind a form of flavin, whether it is riboflavin, flavin mononucleotide (FMN), or flavin adenine dinucleotide (FAD), to sense blue light. In 1987, photolyase was identified as the first photoactive flavoprotein, catalyzing the light-dependent repair of cyclobutane or 6-4 pyrimidine dimers in the DNA of *Escherichia coli* (E. coli). The activation mechanism of photolyase involves electron transfer through a 15 Å triple-tryptophan molecular wire to the FAD cofactor.[11-12] In 1995, cryptochrome, a flavoprotein homologous to photolyase, was discovered to regulate light-induced responses in plants and control circadian rhythms in animals through light perception and magnetic field sensing. The photochemistry of cryptochrome, which involves radical formation, remains an area of active research.[1] A few years later, the first light-oxygen-voltage (LOV) domain was identified in phototropins—plant and algal serine/threonine kinases that respond to blue light to regulate phototropism. In LOV domains, photoexcitation of FMN triggers the formation of a covalent cysteinyl adduct between the C4a position of FMN and a conserved cysteine residue. Around the same time, the first blue light sensor using FAD (BLUF) domain was discovered in a photoactivated adenylyl cyclase (PAC) from a unicellular flagellate, where it regulates photophobic responses. BLUF domains bind oxidized flavin and respond to blue light by undergoing photoexcitation, leading to a reorganization of hydrogen bonding around the chromophore. This structural rearrangement activates or deactivates downstream biological functions.[13] Depending on the specific BLUF protein, the photochemical mechanism may or may not involve radical intermediates.[14]

Structure and function of BLUF proteins

BLUF domain photoreceptors are predominantly found in bacteria, where they play key roles in regulating nucleotide metabolism, phototaxis, photosystem synthesis, and biofilm formation.[15] In most BLUF photoreceptors, the BLUF sensor domain is located at the N-terminus and is linked to an effector domain, with photoexcitation of the flavin chromophore triggering activation of the effector domain. Some of the well-characterized BLUF domains include Activation of Photopigment and PUC Expression A (AppA), PixD (Slr1694), PAC-a, PAC-b, BlsA, BlrB, and BlrP (also referred to as YcgF), with AppA being the most extensively studied among them.[9]

The flavin chromophore in Blue Light Using Flavin (BLUF) domains is bound noncovalently. These domains are intriguing because they utilize subtle rearrangement of hydrogen bonds around the flavin chromophore to transmit signals. All the BLUF domains consist of a ferrodoxin-like module (β1α1β2β3α2β4β5) with two helices aligned parallel to a five-stranded mixed β-sheets (**Figure 1.3**)[9], which form noncovalent interactions with the flavin chromophore. Adjacent to the bound flavin, there are conserved tyrosine and glutamine residues that are sensitive to light in the 380-500 nm wavelength range.

The simplest proposed mechanism for sensing involves a shift in the orientation of the glutamine side chain after light excitation. In the signaling state, this side chain donates a hydrogen bond to the C4=O carbonyl of the flavin isoalloxazine ring and accepts a hydrogen bond from the tyrosine. In the dark state, glutamine donates a hydrogen bond to tyrosine instead. The photocycle of BLUF domains leads to ~10-14 nm red-shifted absorption spectrum (**Figure 1.4**) upon exposure to light. This red shift is attributed to a

rearrangement of hydrogen-bonding interactions between the flavin and the surrounding apoprotein in the signaling state.

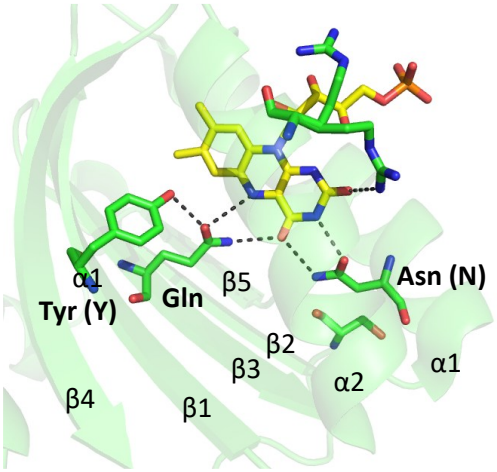

Figure 1.3. Secondary Structure of the BLUF core. The structure of BLUF domain consists of a ferrodoxin-like modules (β1α1β2β3α2β4β5). This figure was made in PyMol using the BLUF domain of OaPAC, PDB: 5x4t.[16]

The initial characterization of the photocycle of a BLUF protein was first reported for AppA.[17] Upon photoexcitation, the absorbance spectrum of AppA undergoes a reversible red-shift of 10 nm. Subsequently, this distinctive behavior has been observed in the absorbance spectra of numerous other BLUF proteins, suggesting that it is a characteristic of all BLUF proteins. The spectral properties observed in the photocycle of AppA distinguish it from other flavin-based photoreceptors like LOV domain and cryptochromes. Furthermore, the dark state recovery kinetics, which involve the transition from the red-shifted state to the dark state, exhibit significant variability among different BLUF proteins, with time scales ranging from a few seconds to several minutes.[18]

While BLUF photochemistry has been extensively studied in the past, understanding the downstream transmission of the blue light signal required a protein system where both the photosensitive domain and the functional domain are covalently linked. OaPAC emerged as a valuable candidate for this purpose since its BLUF domain is directly linked to the C-terminal adenylate cyclase domain. This unique arrangement in OaPAC offers an exceptional opportunity to investigate and decipher the mechanisms involved in transmitting the light signal from the BLUF domain to regulate the activity of the adenylate cyclase domain.

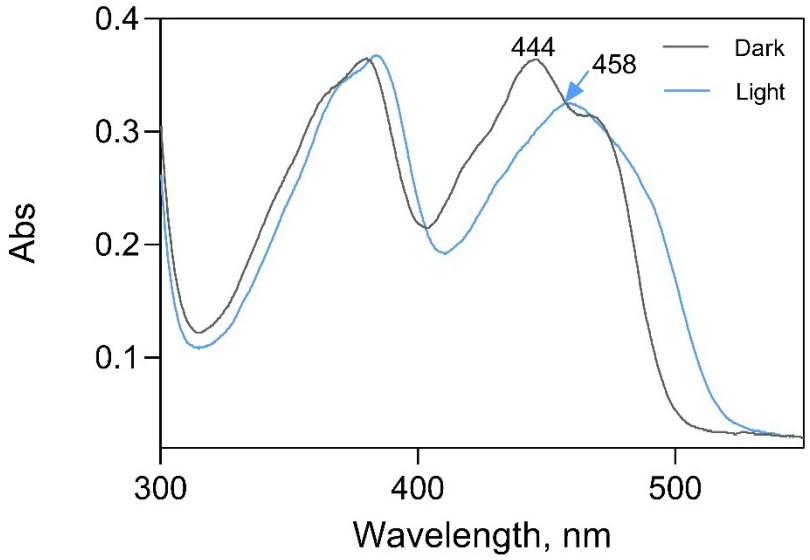

Figure 1.4. UV-Vis spectra of OaPAC BLUF protein. Absorption spectra of flavin bound to BLUF domain protein before (black spectrum) and after (blue spectrum) illumination with 455 nm LED. Photoexcitation of the flavin leads to the light state formation demonstrated by ~ 14 nm red shift and a 493 nm absorption band in UV-Vis difference spectrum.

BLUF proteins catalyzing cyclic AMP production: Photoactivated adenylate cyclases

Second messengers like 3',5'-cyclic nucleoside monophosphates (cNMPs) are pivotal in signal transduction, with cyclic AMP playing diverse roles in bacteria and eukaryotes.[19] Optogenetics, initially used in neuroscience, now extends to cellular processes like cAMP signaling, employing light-regulated enzymes such as photoactivated adenylyl cyclases (PAC).[20] Class III adenylate cyclases, crucial for cAMP generation, require dimerization and specific residue pairs for catalytic activity.[21] BLUF domains, with a flavin chromophore, undergo subtle structural changes upon light absorption, influencing downstream signaling. Bacterial ACs exist as homodimers, forming two catalytic centers at the interface between subunits. In contrast, eukaryotic ACs, including all ten human isoforms, are referred to as pseudoheterodimers. They consist of two complementary catalytic units joined together in a single chain, creating one catalytic center at the subunit interface. The catalytic mechanism of ACs has been extensively studied through biochemical, structural, and computational investigations. Within this mechanism, three pairs of residues play a crucial role. Firstly, a pair of aspartate residues coordinate a divalent metal cofactor, either Mn2+ or Mg2+, which facilitates the nucleophilic attack of the ribose 3'-hydroxyl group on the α-phosphoryl group of ATP. The resulting transition state is stabilized by an arginine and asparagine side chain. The third pair of residues differentiates between ATP and GTP as substrates. In ACs, this pair typically consists of lysine and aspartate, whereas eukaryotic guanylate cyclases (GCs) often have glutamate and cysteine or glutamate and serine in these positions.[21-23]

Numerous studies have focused on characterizing the domain variations among adenylate cyclases (ACs) and extracting insights into their regulatory principles. Although the observed domain architectures did not lend themselves to a meaningful classification and their number

continued to expand with the sequencing of more genomes, functional grouping of the constituent AC domains revealed three main categories: (i) input domains that directly receive stimulation from factors such as intracellular pH, ligand binding, phosphorylation, or light; (ii) transducer domains that transmit signals from upstream input domains or other transducers; and (iii) the AC catalytic domain responsible for generating the second-messenger signal, cAMP. The observed architectural diversity can largely be explained by the modular recombination of input and tranducer domains within this framework, reflecting the role of ACs in converting diverse stimuli into a uniform intracellular cAMP signal. Typically, input domains and transducers are located at the N-terminal region of the proteins, while the catalytic domain is consistently found at the C-terminus. This arrangement closely resembles the organization of other signaling protein families like histidine kinases and diguanylate cyclases. In these proteins, a coiled-coil backbone in the dimeric structure facilitates the propagation of intramolecular signals. This coiled-coil architecture is also compatible with the structure of input and transducer domains, enabling them to undergo conformational changes essential for signal reception and transmission. This observation explains their ability to be combined in various modular architectures.[24]

OaPAC BLUF protein

Photoactivated adenylate cyclase (PAC) is a modular protein identified in *Oscillatoria acuminata*. OaPAC, depicted in Figure 1.5, is a multidomain BLUF protein comprising a BLUF domain that binds FAD, which is covalently connected to an adenylate cyclase domain responsible for catalyzing the conversion of ATP into cAMP and pyrophosphate upon exposure to blue light.[16] The photochemistry of OaPAC is explored in detail in Chapter 2 and 3. The cryogenic crystal structure of OaPAC with ATP bound was elucidated by Chretien et al. OaPAC, linking BLUF domain to adenylate cyclase domain, offers insight into light-mediated signal transmission. Our research combines enzymology, mutagenesis, and unnatural amino acid incorporation to unravel OaPAC's regulation mechanism, promising physiological insights and applications.

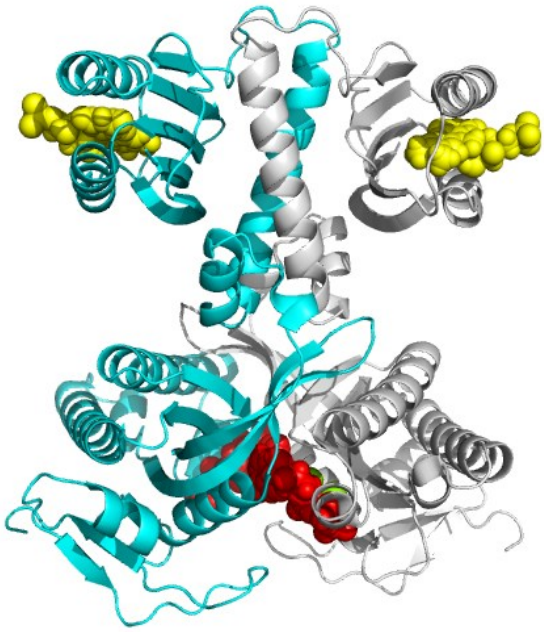

Figure 1.5: Cryogenic crystal structure of OaPAC. The homodimer of full length OaPAC BLUF protein, with FAD (yellow) and ATP (red) bound in the protein, figure made using PyMOL and PDB: 8QFF.[25]

Optogenetics and adenylyl cyclases

Signaling pathways that rel on cyclic nucleotide monophosphates often involve the formation of small areas with high concentrations of these second messengers in a specific time and space. Therefore, tools that enable the precise monitoring and manipulation of intracellular cNMP levels can be valuable in investigating and controlling these pathways. Optogenetics is a versatile approach that allows non-invasive, reversible, and spatiotemporally precise control of cellular processes using light. Although optogenetics originated in neurosciences, it has expanded to include numerous cellular parameters and processes, including cNMP signaling. Optogenetics relies on sensory photoreceptor proteins as genetically encoded, light-regulated actuators. Some natural photoreceptors function as photoactivated adenylyl cyclases (PAC) or guanylyl cyclases that increase cNMP production upon light exposure.[26]

To better understand and improve photoactivated adenylate cyclases, it's important to develop effective assays that can evaluate their enzymatic activity in response to different light conditions.

Chapter 2

Chapter 2: Unraveling the Photoactivation Mechanism of a Light-Activated Adenylyl Cyclase Using Ultrafast Spectroscopy Coupled with Unnatural Amino Acid Mutagenesis

NOTE: The contents of this chapter have been adapted with permission from "Unraveling the Photoactivation Mechanism of a Light-Activated Adenylyl Cyclase Using Ultrafast Spectroscopy Coupled with Unnatural Amino Acid Mutagenesis. Jinnette Tolentino Collado, James N. Iuliano, Katalin Pirisi, **Samruddhi Jewlikar**, Katrin Adamczyk, Gregory M. Greetham, Michael Towrie, Jeremy R. H. Tame, Stephen R. Meech, Peter J. Tonge, and Andras Lukacs; *ACS Chemical Biology* **2022** *17* (9), 2643-2654."

Author Contributions:

SJ, JTC, JNI: Conception and experimental design

SJ, JTC: Samples preparation and handling

SJ, JTC, JNI, KA, KP: Data collection

SJ, JTC: Data analysis and interpretation

JTC, SJ: Drafting the article, critical revision of the article

JTC, SJ: Final approval of the version to be published

GMG, MT, JRHM: Central Laser Facility (CLF) Scientists

All were involved in data analysis and writing of the manuscript.

Introduction:

Adenylyl cyclases (ACs) are an important class of enzymes that catalyze the formation of cyclic adenosine 3′,5′-monophosphate (cAMP) from ATP (**Figure 2.1**). cAMP is a second messenger that plays a crucial signaling role in many organisms, and the photoactivated adenylate cyclases (PACs) represent a subgroup of AC enzymes where the G-protein independent synthesis of cAMP is controlled by light. Early work led to the discovery of PACs in the unicellular flagellate Euglena gracilis (EuPAC),[27,28] and the sulfide-oxidizing bacterium Beggiatoa sp. (bPAC),[29,30] where AC activity is controlled by a blue light using the flavin adenine dinucleotide (BLUF) domain. bPAC was found to have a low activity in the dark and a 100-fold increase in activity upon blue light irradiation.

PACs are attractive optogenetic tools given that the production of cAMP can be controlled by light. For example, EuPAC was expressed in the neurons of the marine gastropod Aplysia enabling photocontrol of neuron stimulation,[31] while bPAC was used in transgenic mice to restore and control the flagellar beat of sperm by light.[32] Another promising PAC (OaPAC) was discovered recently in the photosynthetic cyanobacterium Oscillatoria acuminata which shows the lowest activity in the dark among PAC proteins, enabling finer control of photoinduced cAMP production.[16] OaPAC, **Figure 2.1A**, is a 366-aa residue homodimer comprising an N-terminal BLUF domain and C-terminal AC domain and shows ∼57% sequence homology to bPAC. The full-length structures in both dark and light states were recently reported.[16]

BLUF domain proteins are found in many organisms and are involved in light-dependent processes such as phototaxis, photophobia, and photosynthesis.[33,34] AppA was the first BLUF protein to be discovered and is involved in the light and redox regulation of photosynthetic gene expression in Rhodobacter sphaeroides.[35] Under low light conditions and low oxygen levels, AppA

binds to the transcriptional anti-repressor PpsR. Upon blue light illumination, photoactivation results in a conformational change in AppA that leads to the dissociation of the AppA−PpsR complex enabling PpsR to repress the transcription of genes encoding photosynthetic proteins. The initial event in BLUF photoactivation involves the reorganization of a hydrogen bonding network that surrounds the flavin chromophore resulting in a ∼10 nm red shift of the S0 → S1 flavin transition at ∼450 nm. Site-directed mutagenesis has demonstrated that a conserved tyrosine and glutamine (Y21 and Q63 in AppA) are essential for photoactivation, and there is a general agreement that the red shift in the electronic transition is caused by the formation of a hydrogen bond to the flavin C4=O from the glutamine in the light-adapted state. Early structural studies supported a model which involves a 180° rotation of glutamine,[36,37] and based on experiments on the Slr1694 BLUF domain (PixD), it has been proposed that rotation of the glutamine is triggered by electron transfer from the conserved tyrosine to the flavin.[38] In addition, we have also suggested that the hydrogen bond rearrangement is driven by keto-enol tautomerism of the glutamine,[39,40] a model that is supported by isotope-edited Fourier transform infrared (FTIR) spectroscopy and theoretical calculations.[41,42]

The X-ray structure of OaPAC (PDB: 5x4t) reveals that the flavin binding pocket contains the same conserved residues found in other BLUF proteins.[43] The isoalloxazine ring is surrounded by a conserved tyrosine (Y6), glutamine (Q48), and asparagine (N30), while a conserved methionine (M92) is also present in the flavin binding pocket (**Figure 2.1B**). The semi-conserved tryptophan (W90) is in the Trpout conformation as also noted in the X-ray structure of the BLUF photoreceptor PixD (PDB: 2HFN)[44] and the recently solved X-ray structure of BlsA (PDB: 6W6Z).20 Comparison of the high-resolution crystal structures of wild-type OaPAC in its light

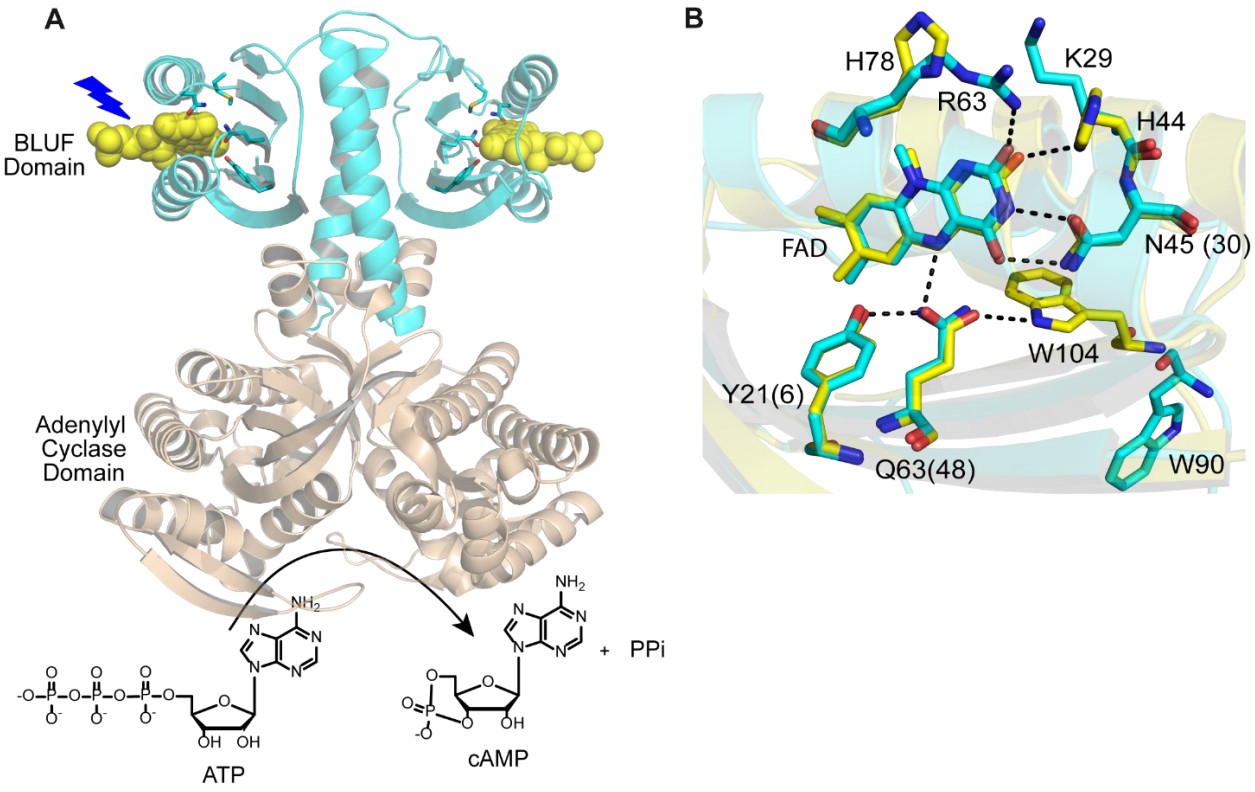

Figure 2.1: The structure of OaPAC and the flavin binding pocket. A. OaPAC is a homodimer composed of a BLUF domain (cyan color) linked to an adenylyl cyclase domain (sand color) responsible for converting ATP to cAMP and PPi in a light-dependent manner (PDB: 5x4t).[43] B. Hydrogen-bonding network that surrounds the isoalloxazine ring of the FAD. The structure of OaPAC (cyan) has been superimposed on the structure of AppA (yellow; PDB: 1YRX) where the tryptophan (W104) is in the Trp_{in} conformation.[37] Residue numbers are for AppA while those in parentheses are for OaPAC.

and dark state reveals that upon light absorption, the Cγ− Cδ bond of glutamine (Q48) rotates about 40°, while the Nε2 atom of the Q48 moves away from N5 of the flavin toward the O4 of the flavin C4=O group enabling a second hydrogen bond to be formed C4=O. Ohki et al.[43] proposed a possible mechanism involving tautomerization of the Q48 side chain and requiring the formation of two radicals, FADH• and Y6• , that would decay within nanoseconds to the signaling state. In this work, we employed fs−ms time-resolved infrared spectroscopy (TRIR) in combination with site directed and unnatural amino acid (UAA) mutagenesis to probe the photoactivation

mechanism of OaPAC, a BLUF protein with a covalently attached output domain. Our studies illustrate that the excitation of FAD in wild-type OaPAC leads to a concerted proton coupled electron transfer (PCET) and the formation of the neutral flavin radical (FADH•) which reacts with Y• radical to form the final light state where the flavin is in the oxidized form. Moreover, we interrogated the role of Y6 in PCET in the activation of wild-type OaPAC by incorporating fluorotyrosine analogues. In the TRIR experiments, only 3-FY6 OaPAC was able to form a light state but with slower kinetics compared to wild-type OaPAC, whereas excitation of 3,5-F2Y6, 2,3,5-F3Y6, and 2,3-F2Y6 OaPAC variants did not generate a detectable light state. In addition, we tested the activity of AC domain for the wild-type OaPAC and n-FY6 variants. Whereas 3-FY6 and 2,3-F2Y6 OaPAC have similar adenylate cyclase activity compared to the wild-type, the 3,5-F2Y6 and 2,3,5-F3Y6 OaPAC variants were inactive.

Methods:

Fluorotyrosine Synthesis using Tyrosine Phenol Lyase (TPL)

The expression and purification of TPL, and the synthesis of n-FY analogues were performed using the method previously reported. For this work, only the 3,5-F_2Y6 and 2,3,5-F_3Y6 were synthesized and purified. Briefly, TPL was expressed and purified from BL21 (DE3) pLysE Escherichia coli (E. coli), and then added to reaction mixtures containing 60 mM sodium pyruvate, 40 μM pyridoxal-5′-phosphate, 30 mM ammonium acetate, 5 mM β-mercaptoethanol and 10 mM the appropriate phenol. After 4 days, the fluorotyrosine analogues were purified, characterized using NMR and mass spectrometry, and lyophilized.

Expression and Purification of Full-Length and BLUF OaPAC

The pCold-I-OaPAC plasmid was transformed into Bl21(DE3) E. coli and grown on an LB-agar plate containing 100 μg/mL ampicillin. A single colony was used to inoculate 10 mL 2x-YT media (Fisher Bioreagents, BP9743-5) containing 100 μg/mL ampicillin which was shaken overnight at 37 °C (250 RPM). Subsequently, the 10 mL culture was used to inoculate 1 L of 2x-YT media in a 4 L flask. The culture was shaken at 37 °C (250 RPM) until the optical density (OD600) reached ~0.8-1. The temperature was lowered to 18 °C, and after 30 min protein expression was induced by adding 0.7 mM IPTG. The cells were harvested after 18 h of induction by centrifugation and the cell pellet was stored at -20 °C until needed. The same protocol was performed for the OaPAC BLUF domain.

The cell pellet containing wild-type OaPAC was thawed and resuspended in resuspension buffer (50 mM NaH2PO4 pH 8.0, 300 mM NaCl). Subsequently, 14 μL of β-mercaptoethanol, phenylmethylsulphonyl fluoride (PMSF, 250 μM final concentration), and ~10 mg of FAD were

added, and the resuspended cells were disrupted using a French Press (Constant Systems Cell Disruptor) at a pressure of 30 kPSI and at 4 °C. The cell debris was removed by centrifugation at 40,000 RPM (185,511 x g) for 1 h at 4 °C, and the supernatant was loaded on to a Ni-NTA column (25 mL containing 5 mL of resin) equilibrated with resuspension buffer. The column was washed sequentially with 100 mL of resuspension buffer containing 0, 5, 10, 20, and 30 mM imidazole, and OaPAC was then eluted using resuspension buffer containing 250 mM imidazole. Fractions containing protein were pooled and immediately exchanged into 20 mM Tris 150 mM NaCl pH 8.0 using a Bioscale P-6 desalting column. Only the protein samples for TRIR measurements were flash frozen with liquid nitrogen (or liquid N_2) and lyophilized. The protein for the assay was used immediately after purification.

Incorporation of Fluorotyrosines using Orthogonal Aminoacyl-tRNA Synthetases

To extend our study to fluorotyrosine analogues with lower pKa values, 3-FY, 2,3-F_2Y, 3,5-F_2Y and 2,3,5-F_3Y were incorporated into position 6 of full-length OaPAC. These analogues are not recognized by tyrosyl–tRNA synthetase and instead were introduced into the protein using E3 and E11, two orthogonal polyspecific aminoacyl-tRNA synthetases. Site-directed mutagenesis was first used to generate a plasmid in which the codon for Y6 was replaced by the TAG stop codon (pCold-I-OaPAC Y6TAG) using pCold OaPAC as template, and the following primers: 5'-GCATATGAAACGCTTAACGtagATCAGCAAATTTTCTCG-3' (forward) 5'-CGAGAAAATTTGCTGATctaCGTTAAGCGTTTCATATGC-3 (reversed). The mutagenesis was verified by the DNA sequencing performed by Genomic Core Facility at Stony Brook University.

The pCold-I-OaPAC Y6TAG plasmid was then co-transformed into BL21(AI) E. coli cells together with either the E3 (for 3-FY, 3,5-F_2Y and 2,3,5-F_3Y) or E11 (2,3-F_2Y) pEVOL plasmid and plated on LB-agar containing both 100 μg/mL ampicillin and 34 μg/mL chloramphenicol to select for cells harboring both plasmids. Subsequently, a single colony was used to inoculate 10 mL of 2xYT media containing 100 μg/mL ampicillin and 34 μg/mL chloramphenicol which was incubated overnight at 37 °C (250 rpm) before 5 mL was then used to inoculate 500 mL of the same media. After 2 h of incubation, 0.05% w/v arabinose was added to induce the expression of the E3 or E11 synthetase. The culture was grown until the OD600 reached ~ 0.4, and 110 mg of the fluorotyrosine analogue in powder form was added to the media to give a final concentration of ~1 mM. The culture was incubated at 37 °C (250 rpm) until the OD600 reached ~1.0, and then the temperature was lowered to 18 °C. After 30 min, 0.7 mM IPTG was added to the media and the cells were harvested after overnight incubation at 18 °C (250 rpm). The n-FY6 samples were purified using the same protocol as that described for the wild-type protein (above). The incorporation of n-FY6 analogue was verified by LC-MS/MS mass spectroscopy.

Light – Dark Steady- State FTIR Difference Spectra

The steady-state spectra were obtained on a Vertex 80v (Bruker) FTIR spectrometer with 3 cm^{-1} resolution and 256 scans. Measured protein samples were in D2O buffer (20 mM Tris 150 mM NaCl pD 8.0) at a concentration of ~0.8 mM and 40 μL was placed between two CaF2 windows with a 50 μm spacer and into a Harrick cell for the measurement. The light adapted state was generated by continuously illuminating the sample using a 455 nm high power mounted LED (Prizmatix, Ltd.) placed in the sample compartment and focused onto the cell. The dark state spectrum was subtracted from the light state spectrum to generate the light minus dark (L-D) difference spectrum. All measurements were performed at room temperature.

Ultrafast Time-Resolved Infrared Spectroscopy

Ultrafast time-resolved IR (TRIR) spectra were measured with ~ 100 fs time resolution at the STFC Central Laser Facility using the ULTRA apparatus described elsewhere.[28,29] TRIR spectra were acquired at 20 °C from 1400 – 1800 cm^{-1} at a resolution of 3 cm^{-1} per pixel. Data were obtained using a 50 μm path length flow cell which was also rastered in the excitation beam to minimize photochemistry (photobleaching, photodegradation and photoconversion). The excitation beam of the 450 nm 100 fs 5 kHz pulses was focused to a spot size of ~ 100 μm and the pulse energy was kept below 400 nJ to avoid build-up of sample in light state. Transient difference spectra (pump on – pump off) were recorded using the IR probe at time delays between 1 ps and 2 ns. After the measurements were recorded the extent of photoconversion was shown to be negligible using absorbance spectroscopy. Spectra were calibrated relative to the IR transmission of a pure cis stilbene standard sample placed at the sample position.

Time Resolved Multiple Probe Spectroscopy (TRMPS)

TRMPS spectra were obtained at 20 °C from 100 fs to 1 ms at the STFC Central Laser Facility. The TRMPS method has been described elsewhere,[29] and previously used by us to analyze the photoactivation of AppABLUF, and other photoactive and photochromic proteins.[27,30-32] Light sensitive samples were analyzed using a rastered flow cell, and data were acquired using a 450 nm pump pulses operated at 0.6-0.8 μJ per pulse and a repetition rate of 1 kHz. The spectral resolution was 3 cm^{-1} and the temporal resolution was 200 fs. A typical measurement was acquired during 45 min of data collection. All samples were prepared at 0.6-0.8 mM concentration in D2O buffer prepared with 20 mM Tris, 150 mM NaCl, pD 8.0. TRIR and TRMPS data were globally analyzed using the sequential model in Glotaran.

Ultrafast Transient Absorption experiments

Ultrafast transient absorption measurements were performed using a Spitfire Ace regenerative amplifier system providing ~800 μJ pulses centered at 800 nm at a repetition rate of 1 kHz. The output of the amplifier was split into a ratio of 1:9. The pulse with the smaller energy was used for generation of the white light continuum probe in a CaF_2 crystal. The higher intensity fraction was frequency doubled to 400 nm and attenuated to ~200-400 nJ/pulse before being used as the pump pulse. The polarization of the probe was again set to a magic angle compared to excitation. To avoid photodegradation the samples were moved with the help of a Lissajous scanner and simultaneously flowed by a peristaltic pump. Absorption changes were measured with an Andor CCD and collected with the help of home written Labview data acquisition software and are again reported as pump on – pump off normalized difference spectra.

Adenylyl Cyclase Assay

The adenylyl cyclase (AC) assay was performed using continuous and discontinuous formats which both monitored the consumption of NADH at 340 nm. In each case the assays were performed on freshly purified protein.

Discontinuous Assay: AC activity was determined at 22 °C in a total reaction volume of 1.5 mL using 20 mM Tris, 150 mM NaCl, 1mM MgCl2 pH 8.0 buffer and by varying the concentration of ATP from 10 μM to 700 μM. The reaction was initiated by adding OaPAC to give a final concentration of 1 μM and 120 μL samples were withdrawn at different time intervals (0, 10, 20, 30, 40, 50, 60, 90, 120, and 180 s) after which they were quenched by heating to 100 °C for 5 min. The reaction mixture was either kept in the dark, for the dark-state control, or continuously illuminated with a blue LED (peak wavelength at 455 nm and excitation intensity of 500 μW per

cm^{-2}) after obtaining the 0 time point sample. After quenching, the samples were then filtered using a 0.22 μm filter (Millipore Sigma, PVDF, 33 mm) and the amount of PPi generated in the reaction was quantified using a pyrophosphate reagent kit from Sigma (P7275), in which the oxidation of NADH to NAD^+ was monitored at 340 nm. This was achieved by combining 66.7 μL of the filtered samples with 33.3 μL of the pyrophosphate reagent in a clear 96 well plate. The plate was incubated for 1 min at 37 °C and then the absorbance at 340 nm was recorded using a BioTek Synergy Neo2 multi-mode plate reader. The absorbance was monitored until no further change was observed, indicating complete conversion of the PPi liberated in the OaPAC reaction to NAD^+. The final A340 for each sample was plotted as a function of time to enable initial velocities to be extracted by fitting the data to a straight line using OriginPro software. The experiment was repeated at multiple ATP concentrations (10 to 600 μM) and Vmax and Km parameters were determined by fitting the initial velocity data obtained as a function of ATP concentration to the Michaelis Menten equation using GraphPad Prism 9 software. A similar protocol was followed for each of the OaPAC n-FY6 variants. For each protein sample, the experiment was performed in duplicates and the average of data plotted with the standard error of the mean (SEM). Continuous assay: Samples were prepared as described above except that the production of PPi was directly monitored by combining 250 μL of the pH 8.0 OaPAC/ATP reaction mixture with 125 μL of the reconstituted pyrophosphate reagent before illuminating the sample with light. The reaction mixture was incubated in a water bath at 30 °C for 1 min then 100 μL was placed in a sub micro quartz cuvette. Using an Ocean Optics USB2000+ spectrometer, the absorbance at 340 nm was recorded for 40 s before the sample was illuminated using the blue LED (see above). The reaction was continuously monitored for at least 4 min and initial velocities were extracted for each ATP concentration from a plot of A340 vs time. Values for Vmax and Km were calculated by fitting the initial velocity

data obtained as a function of ATP concentration to the Michaelis Menten equation using GraphPad Prism 9. The same steps were performed for the n-FY6 variants, however for the 2,3-F2Y6, 3,5-F2Y6 and 2,3,5-F3Y6 variants a background rate in the presence of blue light and in the absence of ATP was observed, which was subtracted from the initial velocities obtained in the presence of ATP. The data reported for the continuous assay are the averaged mean of 2 replicates with their standard error of the mean (SEM).

Results and Discussion:

UV-visible absorption and FTIR difference spectra of wild-type OaPAC

Figure 2.2A shows the steady-state absorption spectrum of wild-type OaPAC obtained before and after irradiation with 450 nm blue light LED (~500 μW of 455 (±10) nm light, 20 s illumination). The wild-type protein exhibits a 14 nm red shift in the flavin absorption spectrum upon blue light irradiation, which is a characteristic of all photoactive BLUF proteins and is due to changes in hydrogen bonding around the flavin. The absorption difference spectrum (**Figure 2.2A**, blue spectrum) shows an absorbance maximum at 493 nm, associated with light-state formation. Once illumination is discontinued, the absorption spectrum relaxes back to that observed for the dark-state with a time constant of ~5 s (**Figure 2.2B**). The rate of dark-state recovery for OaPAC is faster than that reported for other BLUF proteins including PixD (45 sec), $AppA_{BLUF}$ (23 min) and BlsA (8 min).[45,46]

The structural changes that accompany light-state formation were first studied using steady-state FTIR difference spectroscopy. The difference spectrum of OaPAC was generated by subtracting the dark state FTIR spectrum from that obtained while the sample was continuously illuminated with 460 (±5) nm LED (Prizmatix, Ltd.) placed in the sample compartment and focused onto the cell using an objective. The light minus dark (L-D) IR difference spectrum from 1800-1100 cm^{-1} is shown in **Figure 2.2C**, where positive and negative bands are attributed to the light-induced and ground state vibrational modes, respectively. At higher wavenumbers, the L-D difference spectrum of wild-type OaPAC is similar to that observed for other BLUF proteins where two prominent bands at 1692(+)/1703(-) cm^{-1} are assigned to a shift in the C4=O carbonyl vibration of the flavin, consistent with an increase in hydrogen bonding in the light-state.[39,47] The lower wavenumber modes in the 1550 to 1650 cm^{-1} region are assigned to changes in the vibrations of

the protein backbone, in particular the β5 strand which is important for signal transduction.[29,48,49] The difference spectrum of the OaPAC BLUF domain lacking the AC domain (1-141 aa; $OaPAC_{BLUF}$), was also acquired and exhibits significantly lower intensity in the difference bands between 1550 to 1650 cm^{-1} region, especially at 1627 cm^{-1} (**Figure 2.2C**). Thus, compared to the full-length protein, the light-induced structural changes of the protein backbone in the $OaPAC_{BLUF}$ are suppressed. A similar observation was reported in the comparison of light-induced structural changes in the full-length protein and BLUF domain of the cyclic-di-GMP phosphodiesterase YcgF/Blrp.[49] In addition, a similar study was also performed on the full-length and isolated BLUF domain of bPAC. Interestingly, a large positive signal was observed in the frequency range expected for α-helical amide I vibrations around 1650 cm^{-1} in the full-length bPAC, suggesting that the photoactivation of the cyclase domain involves the formation of helical structures. In the FTIR difference spectrum of wild-type OaPAC, we do not observe a positive peak in the 1650 cm^{-1} region, indicating that light induced structural changes of wild-type OaPAC might differ from bPAC in the signal transduction mechanism. This is not unexpected as the C-terminal region of bPAC is shorter compared to OaPAC; interestingly, the shorter C-terminal region in bPAC results in a more efficient cAMP production compared to OaPAC.[50]

TRIR and TRMPS of wild-type OaPAC

Figure 2.3 shows the temporal evolution of the TRIR spectra of the dark-adapted wild-type OaPAC upon excitation of the isoalloxazine chromophore by a 450 nm sub-100 fs pump pulse.

The TRIR difference spectra are comprised of negative and positive bands, where the negative bands (bleaches) are associated with depletion of the isoalloxazine singlet ground state, or with changes in the vibrational spectrum of the surrounding protein occurring either instantaneously as a result of chromophore excitation or due to subsequent structural dynamics.[51]

The positive bands (transient absorptions) arise due to vibrations of the electronically excited states of isoalloxazine, or to amino acid modes perturbed by electronic excitation, or to vibrational modes of products formed following excitation.

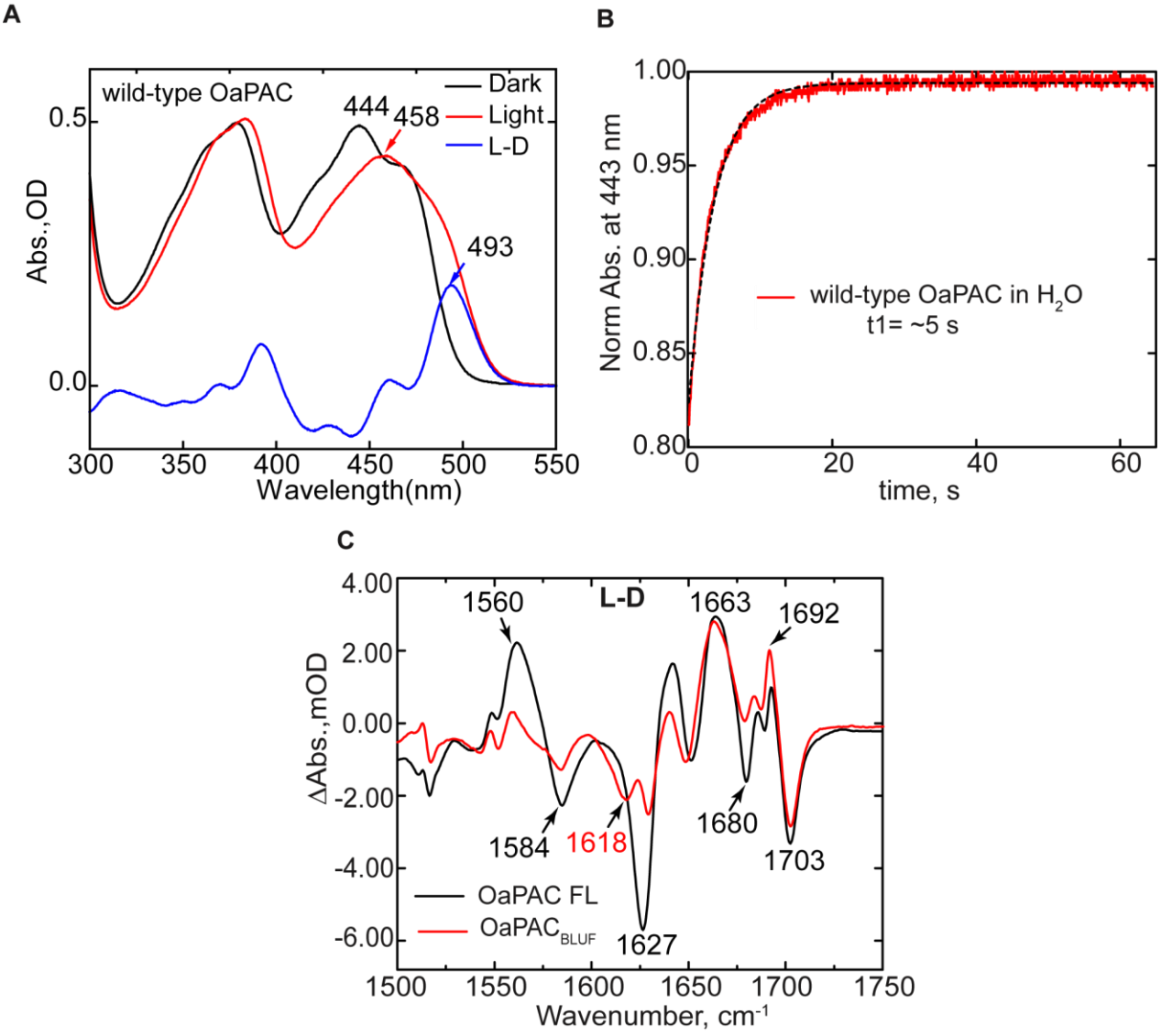

Figure 2.2 UV-visible absorption and FTIR difference spectra of wild-type OaPAC. A. Steady-state absorption spectra for wild-type OaPAC in the dark and light. B. Dark state recovery of the band at 444 nm which has a time constant of ~5 s. C. Comparison of the steady-state IR difference spectrum of full-length OaPAC (OaPAC FL) with $OaPAC_{BLUF}$. The FTIR difference spectrum was obtained using 1 mM protein in a 50 µm CaF_2 cell. The L-D spectrum was generated by subtracting the IR spectrum of OaPAC acquired before irradiation from the spectrum acquired while the sample was irradiated using a 455 nm mounted LED for at least 20 s.

TRIR spectra of wild-type OaPAC (**Figure 2.3A and 2.3B**) are broadly similar to spectra of the other BLUF domain proteins we and other have previously studied.[48,52-54] **Figure 2.3B** shows the evolution associated difference spectra (EADS) which represent the spectral evolution over time. To generate the EADS, TRIR data (**Figure 2.3A**) were globally analyzed in Glotaran using a sequential decay model of 4 components in which three of the lifetime components were allowed to vary while the 4th component was kept constant (indicating a product with effectively infinite lifetime) yielding three-time constants of 3.9 ps, 24 ps and 184 ps (**Table 2.1**). The first EADS (**Figure 2.3B**, black line) shows the instantaneously formed excited state of FAD (FAD*) in wild-type OaPAC. The excited state is characterized by transient bands at 1383 and 1420 cm^{-1}, and ground state bleaches at ~1546, ~1664 and ~1704 cm^{-1}, which are assigned to the C10a−N1, C2=O and C4=O flavin modes, respectively.[53,55] The first EADS also shows a band at 1520 cm^{-1}, indicating that the $FAD^{\bullet-}$ intermediate is formed at very early times post excitation (**Figure 2.3A, inset**).[56,57] The second EADS (**Figure 2.3B,** red spectrum) forms with a 3.9 ps time constant and shows that FAD* is decaying while the ground state is already recovering. Significantly this spectrum is characterized by the appearance of a new transient at ~1528 cm^{-1} which is a vibrational marker for the neutral semiquinone $FADH^{\bullet}$ species (NSQ) that is also observed in flavodoxin and glucose oxidase.[57,58] In EADS3, the $FADH^{\bullet}$ transient at 1528 cm^{-1} increases in amplitude with a time constant of 24 ps and relaxes in 184 ps. On this timescale the FAD* continues to decay, consistent with the complex multiexponential kinetics observed in other BLUF domains,[54] and there is a similarly complex evolution in the region of the FAD C=O bleach modes, suggesting underlying dynamics in protein modes. Simultaneously with $FADH^{\bullet}$ formation and decay, we observe formation of another transient at 1635 cm^{-1} coinciding with an increase of a bleach at 1623 cm^{-1}. The 1623 (-)/1635 (+) cm^{-1} modes can correspond to another flavin radical mode and/or a

tyrosine radical.[57] The fourth EADS (**Figure 2.3B**, green line) represents the final non-decaying component which is formed around 184 ps. The main feature in EADS4 is the formation of the transient at ~1694 cm^{-1}, which reflects the formation of the light state; this vibrational mode is assigned to the C4=O vibration of the flavin. The downshift from 1704 cm^{-1} to 1694 cm^{-1} reflects the reorganization of the hydrogen bonds around the flavin after light excitation and the decrease in frequency is consistent with the formation of a second hydrogen bond to C4=O.

For wild-type OaPAC, the time scale of TRIR is not sufficient to observe the full evolution of the protein modes leading to the final light-state, thus we also performed time-resolved multiple probe spectroscopy (TRMPS) to further monitor the protein dynamics. Superimposition of the 3 ns TRIR spectrum with the 100 μs TRMP spectrum and the steady-state FTIR difference spectrum, reveals that while the important changes in the steps of photowhcycle dynamics have occurred within the first 3 ns, further evolution occurs beyond 100 μs which exceeds the time window of TRMPS instrumentation and is likely due to secondary structural changes in the AC domain, most notably in the 1550-1660 cm^{-1} region. Tokonami et al. performed transient absorption measurements on the full-length OaPAC and observed a slow reaction phase in the tens of milliseconds reflecting a conformational change at the C-terminus domain, which is consistent with this result.[59]

Time-dependent evolution of TRIR bands

To gain further insight into the structural dynamics of photoactivation, we determined the kinetics for the time-dependent evolution at the wavenumbers of some of the key transients and bleaches in the TRIR spectra (**Figure 2.4**). The kinetic traces of the raw data are shown as dots while the fit recovered from Global analysis is shown by dashed lines. In **Figure 2.4A,** the excited state of the flavin, represented by the 1383 cm^{-1} transient, decays more rapidly than the rate of

ground state recovery (1546 cm^{-1} bleach), indicating that relaxation of the excited-state involves intermediate species that precede reformation of the ground-state. The intermediate species formed are flavin radicals, and in **Figure 2.4B**, we compare the kinetics of the two flavin radical intermediates, $FADH^{\bullet}$ and $FAD^{\bullet-}$, to show that they are both forming at the similar time, indicating that the electron and proton transfer is not sequential, but rather that concerted proton-coupled electron transfer is occurring. Furthermore, we compared the kinetics of $FADH^{\bullet}$ at 1528 cm^{-1} with the transient at 1635 cm^{-1} which demonstrates that both species evolve with the same rate constant (**Figure 2.4C**), suggesting that the 1635 cm^{-1} vibrational mode is also marker for the $FADH^{\bullet}$ state of the flavin. In addition, the transient observed at 1694 cm^{-1} (**Figure 2.4D**) reflects the formation of the second hydrogen bond to the flavin C4=O group found in the light-state with a time constant of 184 ps.

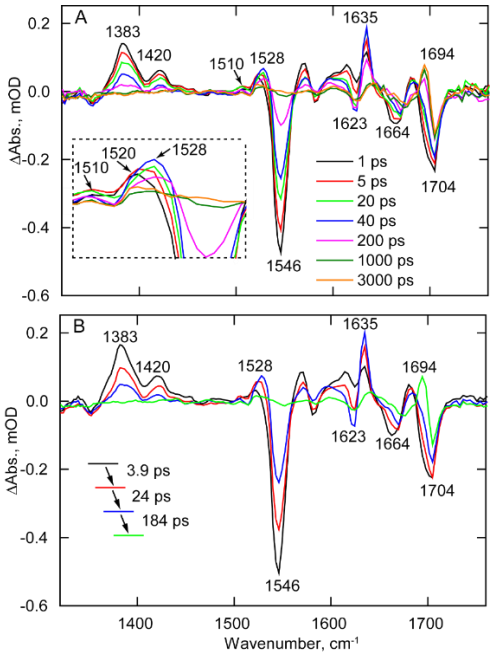

Figure 2.3. TRIR Spectra of the Wild-type OaPAC Dark State. A. Temporal evolution of wild-type OaPAC spectra recorded between 100 fs and 3 ns after 450 nm excitation. B. Evolution associated difference spectra (EADS) of wild-type OaPAC obtained from a global fit of the TRIR data in A. Transients assigned to $FADH^{\bullet}$ (1528 cm^{-1}), $FAD^{\bullet-}$ (1520 cm^{-1}) and $Tyr^{\bullet}$ (1510 cm^{-1}) are shown in the inset.

Table 2.1. Time constants from TRIR data for wild-type OaPAC and n-FY6 OaPAC variants

	τ_1/ps	τ_2/ps	τ_3 /ps
wild-type OaPAC[a]	3.9	24	184
3-FY6 OaPAC[a]	3.1	32	510
2,3-F_2Y6 OaPAC[b]	52	2079	infinite
3,5-F_2Y6 OaPAC[b]	21.5	1354	infinite
2,3,5-F_3Y6 OaPAC[b]	117	1682	Infinite

[a]The TRIR data of wild-type OaPAC and 3-FY6 OaPAC were globally analysed in Glotaran using three-time constants to adequately describe the data.

[b]For 2,3-F_2Y6, 3,5-F_2Y6 and 2,3,5-F_3Y6 OaPAC, only two-time constants were used to fit the data followed by an "infinite" lifetime extending beyond the time scale of the TRIR measurements.

The photocycle of OaPAC can be compared with that observed for other BLUF proteins. For instance, in PixD the anionic radical ($FAD^{\bullet-}$) transient at 1515 cm^{-1} is formed in 2.5 ps and then starts to decay around 20 ps followed by the appearance of the $FADH^{\bullet}$ transient at 1535 cm^{-1} with a time constant of 110 ps. Thus, the formation of the two radical species in PixD are well separated in time and formed sequentially following the $FAD^* \rightarrow FAD^{\bullet-} \rightarrow FADH^{\bullet}$ photocycle, which is also observed in other photoactive flavoproteins such as the cryptochrome superfamily.[60,61] However, in wild-type OaPAC we observe a transient at 1520 cm^{-1} which we suggest has contributions from both flavin radicals ($FAD^{\bullet-}$ and $FADH^{\bullet}$). The presence of an $FADH^{\bullet}$ population is supported by the appearance of the transient at ~ 1510 cm^{-1} at early times

which can be assigned to a neutral tyrosine radical.[58] Therefore the FADH$^{\bullet}$-Tyr$^{\bullet}$ radical pair is formed very fast after excitation. This assumption is in harmony with the photoactivation model proposed by Ohki et al.[43] The presence of the 1520 cm^{-1} transient suggests that there are two possible (parallel) electron transfer routes where the anionic and neutral flavin radical can be formed at the same time. As we discuss later, replacement of Y6 with F-Tyr residues halts the photocycle at FAD$^{\bullet-}$ resulting in a clearly observed transient at 1515 cm^{-1}.

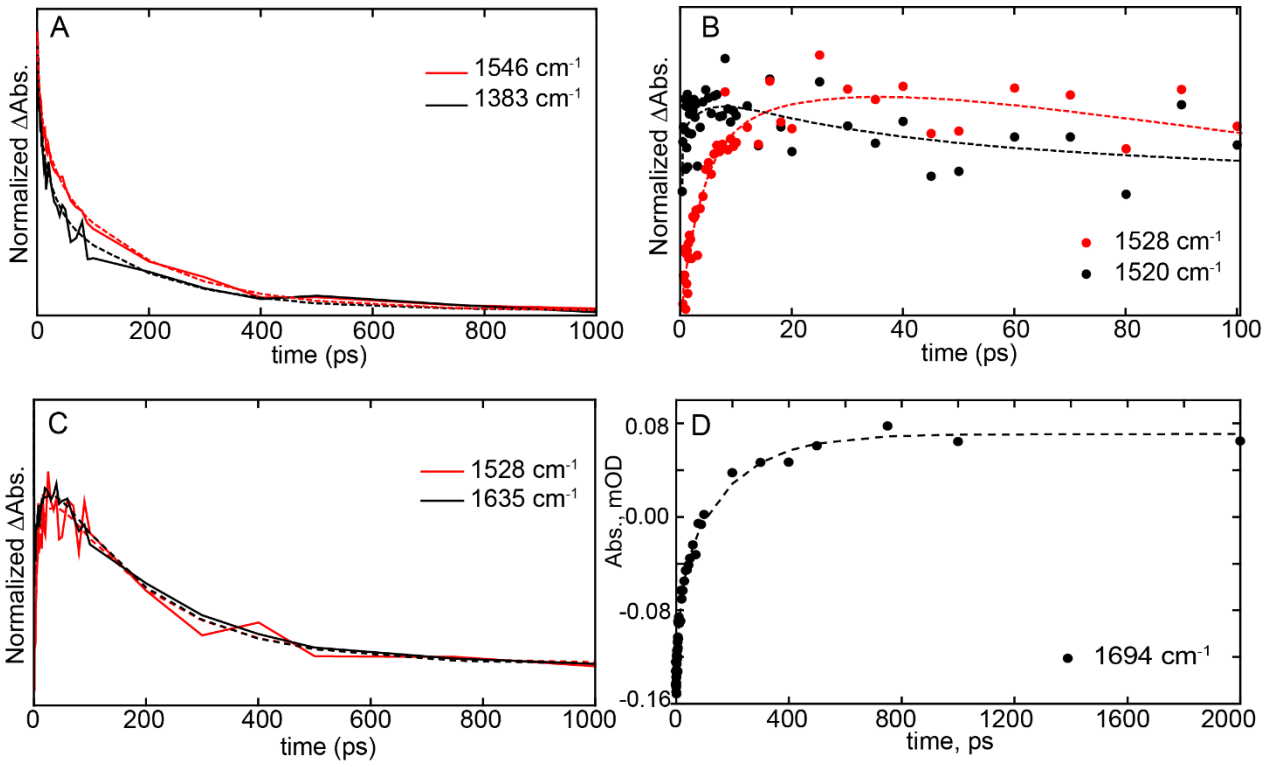

Figure 2.4. **Time-dependent evolution of TRIR bands**. A. Kinetic traces of the excited state decay (1384 cm^{-1}) and the ground state recovery (1546 cm^{-1}, shown inverted for comparison). B. Comparison of the rise and decay of radical intermediates in wild-type OaPAC. C. Comparison of the rise and decay of radical transient at 1528 cm^{-1} with transient evolving at 1635 cm^{-1}. D. Kinetic trace of the 1694 cm^{-1} transient, assigned to light state formation. Raw data are shown as solid lines or dots, while global fitting results are shown as dashed lines.

Visible transient absorption spectroscopy

TA measurements of wild-type OaPAC were also performed in the visible range to obtain additional information on the photoactivation mechanism (**Figure 2.5**). Similar to the TRIR spectra, global analysis of the TA measurements reveals three dominant EAS (Evolution Associated Spectra) which have been analyzed by spectral fitting. The first 5 ps EAS can be assigned to the decay of the oxidized flavin excited state (FAD^{*}-FAD_{ox}), which evolves to the next EAS (red line) with a lifetime of 83 ps (**Figure 2.5B**). Besides the absorption band at ~505 nm, the second EAS component shows a decrease of the stimulated emission band at 550 nm, partial loss of the ground state bleach and a shoulder at ~490 nm. EAS2 strongly resembles the spectrum of a neutral semiquinone flavin radical, $FADH^{\bullet}$,[62] and the spectral fitting reveals substantial contributions from $FADH^{\bullet}$. The non-decaying EAS (final or asymptotic spectrum, blue line), which has been extrapolated to 1 µs, shows the disappearance of the ground-state bleach, and the appearance of an absorption feature near 488 nm. This non-decaying component is modelled as the difference of the light-adapted and dark-adapted linear absorption spectra of wild-type OaPAC.

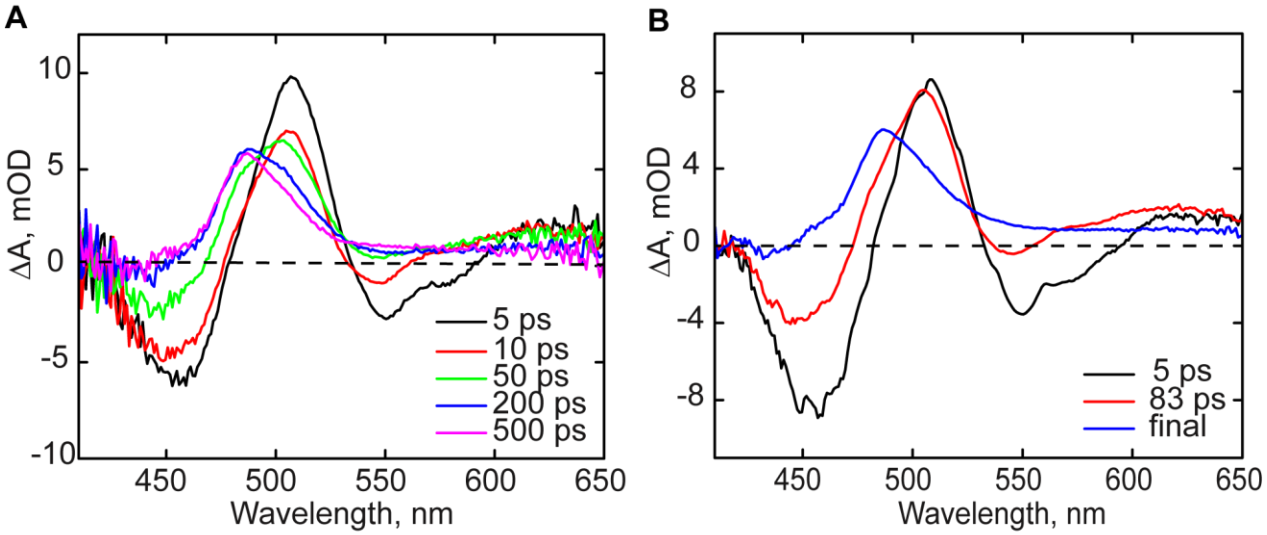

Figure 2.5. Transient absorption spectra of wild-type OaPAC. A. Spectra recorded at different time delays. B. EAS spectra of wild-type OaPAC determined by global analysis.

Mutagenesis of Y6 and W90 to investigate the electron donor in wild-type OaPAC

Photoactivation of OaPAC involves an ultrafast electron transfer to the flavin following excitation (**Figure 2.3**). Although the conserved tyrosine (Y6) is thought to be the primary electron donor, the adjacent tryptophan W90 could also function as a competitive source of electrons. To explore this possibility, we constructed the Y6F and W90F OaPAC mutants and characterized their photophysical properties. Phenylalanine is not expected to function as an electron donor to FAD*.[58] Although the Y6F mutant is photoinactive, irradiating Y6F leads to the fully reduced form of the flavin forming ($FADH^-$). This behavior is different from the Y7F bPAC mutant where the neutral semiquinone is formed upon blue light illumination.[29] The W90F mutant is however still able to form a light-state albeit with a ~5-fold reduction in the rate of dark state recovery.

Even though Y6F does not form a (meta) stable light state in the UV-vis measurement, the TRIR data indicate a sequential formation of $FAD^{\bullet-}$ (1518 cm^{-1}) followed by $FADH^{\bullet}$ (1528 cm^{-1}). A transient is also observed at 1488 cm^{-1} which is consistent with the presence of a tryptophan cation radical ($TrpOH^{\bullet+}$), suggesting that W90 can act as an electron donor in the absence of Y6.[58] This is in agreement with studies by Gauden et al. who demonstrated that W104 in AppA can act as an electron donor albeit via a pathway that does not contribute to the light sensing of AppA.[63] In addition, Ishikita calculated that the redox potential of W104 in the dark and light adapted states is as high as 1.133 V and 1.116 V, respectively, assuming a configuration in which the tryptophan is oriented away from the flavin.[64] Thus, the tryptophan that is found adjacent to the flavin in most BLUF proteins (W104 in AppA, W91 in PixD, W90 in OaPAC), is fully able to function as an electron donor.

The TRIR spectra of Y6F thus show that mutation of the conserved tyrosine does not abolish electron transfer, and that formation of radical species occurs sequentially, as observed in

PixD,[54] but on a substantially longer timescale. First the formation of the anionic flavin radical ($FAD^{\bullet-}$) at 1518 cm^{-1} occurs in 16 ps followed by formation of the neutral ($FADH^{\bullet}$) flavin radical at 1528 cm^{-1} in ~ 100 ps. As expected, there is no transient observed at 1694 cm^{-1} as a light-adapted state is not formed in this mutant. The tryptophan (W) at position 90 is expected to be the electron donor since the primary electron donor (Y6) is absent. Indeed, formation of the 1488 cm^{-1} peak reflects the formation of the tryptophan cation radical ($TrpOH^{\bullet+}$),[58] which is again consistent with the fact that removing Y6 leaves W90 as the only electron donor. The Y to F mutation was also introduced into PixD (Y8F),[54] however, unlike OaPAC, the TRIR data show that Y8F PixD mutant was only able to participate in one transfer process, either electron transfer (ET) or proton transfer (PT) since the rise and decay of the signal at 1515 and 1530 cm^{-1} had the same kinetics.[54]

The TRIR spectra of W90F OaPAC reveal the formation of the flavin neutral radical species ($FADH^{\bullet}$) as seen in the wild-type protein. The peak observed at 1512 cm^{-1} reflects the formation of the neutral tyrosine radical as in the case of wild-type OaPAC.[58] In addition, the W90F mutant contains the same pair of modes observed in the wild-type at 1621 (-)/1631 (+) cm^{-1}, as well as the 1693 cm^{-1} the vibrational mode which is associated with the formation of the light state.

TA measurements of W90F mutant were also performed in the visible range and compared to wild-type OaPAC. Similar to the wild-type, global analysis of the TA measurements reveals three dominant EAS which have been analyzed by spectral fitting. The first EAS of W90F resembles that observed in wild-type OaPAC and is dominated by the excited state of the flavin and corresponding ground state bleach. A striking difference is observed in the 520-570 nm region of the second EAS where one can see a larger positive feature compared to the wild-type data. Spectral fitting of EAS2 shows that in the case of this mutant we have a larger contribution from the neutral semiquinone ($FADH^{\bullet}$). This suggests that the proton coupled electron transfer process

is more efficient in the W90F mutant compared with the wild type as the removal of the adjacent tryptophan eliminates the alternate electron transfer route. This difference between the wild-type and W90F mutant was not obvious in the TRIR data, however, the TA data shows that the decay of the excited state at 510 nm for W90F is faster than wild-type indicating that the PCET process is more efficient in the mutant.

Effect of Y6 fluorination on the photocycle of OaPAC

Y6 is a strictly conserved residue in all BLUF domain proteins and is critical for photoactivity since replacement of this residue with any other amino acid including phenylalanine yields a photoinactive protein. The role of tyrosine as an electron and/or proton donor is pH dependent, and the phenol pKa varies depending on whether phenolic hydroxyl group on tyrosine is reduced (pK_{red}) or oxidized (pK_{ox}). For tyrosine in solution, pK_{red} and pK_{ox} have values of 9.9 and -2, respectively, and above pH 9.9 tyrosine deprotonates to form tyrosinate (Y^-) so that electron transfer generates the neutral tyrosine radical ($Y^\bullet$). At pH values between pK_{red} and pK_{ox} tyrosine is protonated and the $Y^\bullet$/Y redox couple has a pH dependent potential that increases by 59 mV per pH unit. Finally, if the pH is more acidic than pK_{ox}, electron transfer will generate the cation radical ($Y^{\bullet+}$).[65]

In order to explore the role of the tyrosine pKa on OaPAC photoactivation, we thus replaced Y6 with fluorotyrosine (F-Tyr) analogues to modulate the acidity of the phenol. In contrast to tyrosine (pKa 9.9), 2,3,5-F_3Tyr has a pKa of 6.4 and is therefore ~3,000-fold more acidic than tyrosine with a reduction potential ($Y^\bullet/Y^-$) that is ~200 mV higher. LC-MS/MS analysis did not detect any native tyrosine in the F-Tyr-substituted proteins, indicating that the F-Tyr content of each variant was ≥ 99%.

Electronic state of n-FY6 variants**:** We first examined the electronic absorption spectrum of the n-FY6 OaPAC variants before and after illumination. As observed in **Figure 2.6**, all the n-FY6 variants have a λ_{max} at 444 nm which is the same as the electronic spectrum of the flavin in wild-type OaPAC, suggesting that the fluorotyrosine analogues have not dramatically perturbed the flavin binding pocket. However, irradiation of each variant only caused a detectable red shift in

the flavin absorption for the 3-FY6 and 2,3-F_2Y6 OaPAC proteins. The shifts were 10 nm and ~5 nm, respectively, whereas no red shift was observed for either 3,5-F_2Y6 or 2,3,5-F_3Y6 OaPAC within the 10 ms time resolution of the experiment. These results indicate that lowering the pKa impacts the stability of the light state.

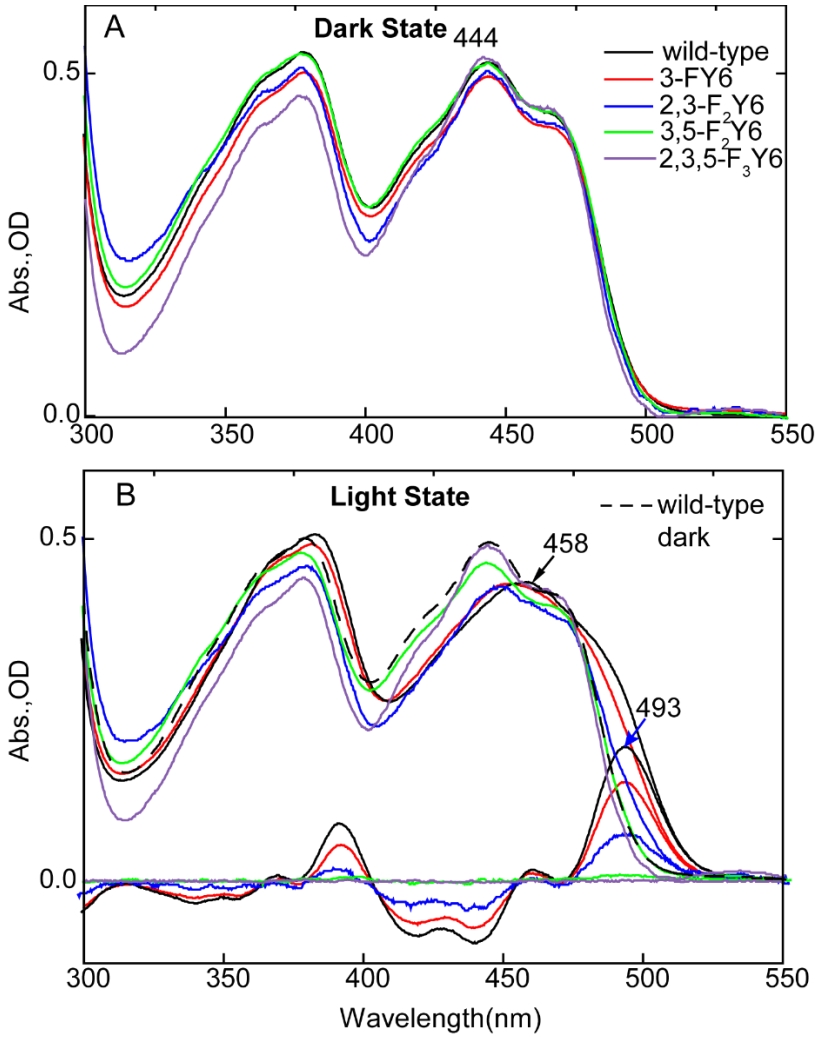

Figure 2.6. Electronic spectra of n-FY6 OaPAC Variants in H_2O. Comparing the dark (A) and light (B) state absorbance spectra of n-FY6 variants to wild-type OaPAC, the flavin electronic state is not perturbed by the fluorotyrosine. Only 3-FY6 and 2,3-F_2Y6 forms a red-shifted spectrum upon illumination of sample with 450 nm LED, and both have a difference electronic spectrum illustrating an absorbance of the light state at 493 nm.

FTIR Steady-State Difference Spectra of the n-FY6 OaPAC variants: The FTIR steady-state difference spectra of each OaPAC n-FY6 variant is compared with wild-type OaPAC in **Figure 2.7**. Only the difference spectrum of the 3-FY6 variant resembles wild-type OaPAC. Three difference modes at ~ 1663 (+), and 1692 (+)/1703 (-) cm^{-1}, previously assigned to the C4=O carbonyl of the flavin, are conserved in the FTIR difference spectrum of the 3-FY6 OaPAC. The bleaches at 1584 and 1627 cm^{-1} are also observed which are assigned to protein backbone modes. However, the magnitude of the light-induced structural change is smaller than observed in the wild-type photoreceptor.

The FTIR difference spectra of the 2,3-F_2Y, 3,5-F_2Y, and 2,3,5-F_3Y variants differ the most from wild-type OaPAC in the region of 1500-1650 cm^{-1}. Although a small change can be observed around the C4=O carbonyl of flavin (1694 (+)/1703 (-) cm^{-1}), only minimal changes are observed in the protein backbone marker modes in the 1600 cm^{-1} region. Compared to 3,5-F_2Y, and 2,3,5-F_3Y variants, the difference spectrum of 2,3-F_2Y6 variant shows the most light-induced changes in the protein backbone modes (1584 and 1627 cm^{-1}). Interestingly, the 2,3,5-F_3Y6 sample has two modes at 1531 (-)/1547 (+) cm^{-1} that are not observed in the wild-type protein but are found in the other n-FY6 analogues, albeit with lower intensity.

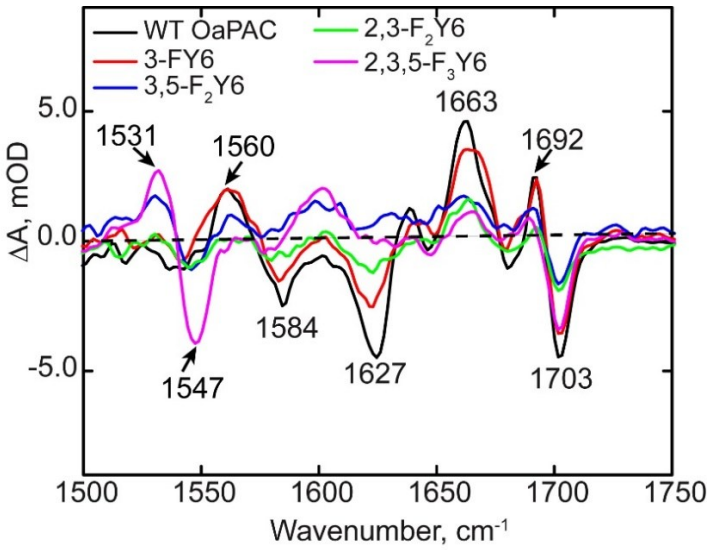

Figure 2.7. FTIR difference spectra of wild-type OaPAC and n-FY6 analogues. Only the L-D difference spectrum of the 3-FY6 resembles the wild-type protein.

Analysis of n-FY6 OaPAC photoactivation using TRIR and TRMPS: The forward photoactivation reaction of the n-FY6 OaPAC variants was studied using ultrafast time-resolved infrared spectroscopy (TRIR) and time-resolved multiple probe spectroscopy (TRMPS). **Figure 2.8** depicts the temporal evolution of 3-FY6, 2,3-F_2Y6, 3,5-F_2Y6 and 2,3,5-F_3Y6 OaPAC variants. At 1 ps, all the variants contain the same transients and bleaches as the wild-type protein. For instance, transients assigned to the excited state of FAD are observed at 1383 and 1420 cm^{-1}, while bleaches at 1546, ~1660 and 1704 cm^{-1} are also present, which are assigned to the ground state of FAD, C2=O and C4=O, respectively. However, as the TRIR spectra evolve over time, significant differences are observed compared to the wild-type protein. The TRIR spectra of 3-FY6 OaPAC most closely resemble the wild-type spectrum although the evolution of the transients and bleaches occurs 5-fold slower. Formation of the radical intermediate $FADH^{\bullet}$ is observed at 1525 cm^{-1} in 3-FY6 OaPAC, suggesting that this variant is still able to participate in PCET. However, the amplitude of the radical signal is smaller in 3-FY6 OaPAC. In addition, the differential line shape

at 1623 (-)/1635 (+) cm^{-1}, observed in wild-type OaPAC is not as pronounced in the 3-FY6 mutant and the bleach is shifted by 5 cm^{-1} from 1623 cm^{-1} to 1628 cm^{-1}. Finally, the light state, characterized by the transient at 1694 cm^{-1}, forms with a time constant of 510 ps, which is much slower than in wild-type OaPAC (184 ps).

The photocycle of the other n-FY6 variants, 2,3-F_2Y6, 3,5-F_2Y6 and 2,3,5-F_3Y6, does not proceed beyond $FAD^{\bullet-}$ (transient observed at 1515 cm^{-1}), thus no transients are observed at 1528 cm^{-1} for $FADH^{\bullet}$ and at 1694 cm^{-1} for the light state (**Figures 2.8**). In addition, these variants lack the 1623 (-)/1635 (+) cm^{-1} modes observed in wild-type and 3-FY6 OaPAC. The kinetics of the excited state decay at 1383 cm^{-1} and ground state recovery at 1546 cm^{-1} are much slower compared with wild-type OaPAC (**Table 2.1)**. Finally, the TRIR data contain a feature around 1490 cm^{-1}, indicative of triplet state formation which is absent in the wild-type OaPAC.

Time-resolved multiple probe (TRMPS) spectra were also obtained for all the n-FY6 variants to investigate whether further evolution occurs beyond the timescale of TRIR (3 ns). The TRMPS data confirm that only 3F-Y6 OaPAC forms a light state whereas the 2,3-F_2Y6, 3,5-F_2Y6 and 2,3,5-F_3Y6 OaPAC do not have an observable or detectable transient at 1694 cm^{-1}. In addition, the transient at 1490 cm^{-1}, assigned to a triplet state mode of the flavin, is more distinguishable in all n-FY6 variants compare with wild-type where no transient is observed.

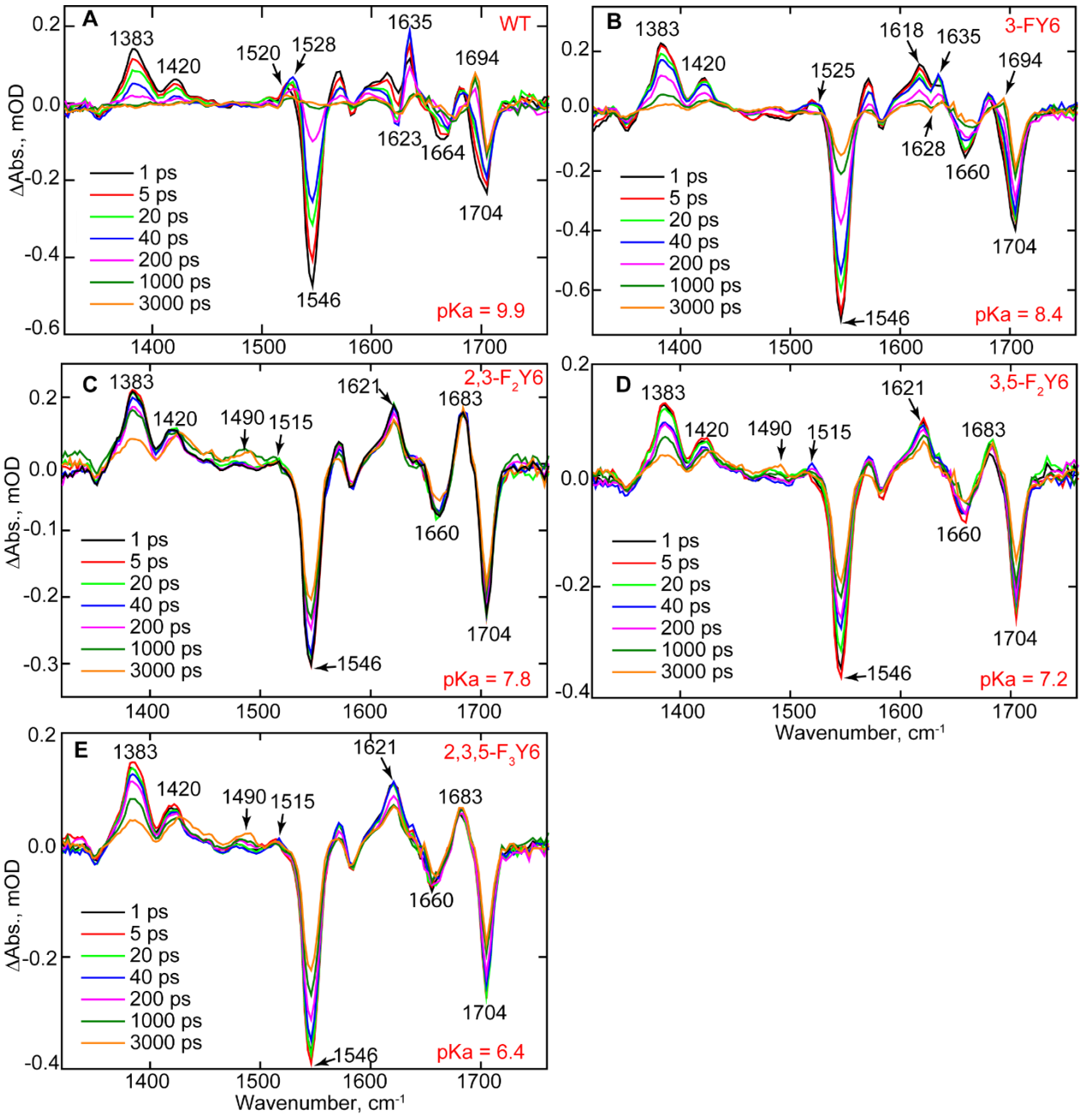

Figure 2.8. TRIR of wild-type OaPAC and the n-FY6 OaPAC variants. Spectra recorded at 1, 5, 20, 40, 200, 1000, and 3000 ps are shown in the Figure. A. wild-type (WT), B. 3-FY6, C. 2,3-F_2Y6, D. 3,5-F_2Y6 and E. 2,3,5-F_3Y6.

Adenylate Cyclase Activity

An enzymatic assay was performed to examine the impact of modulating the pKa and/or reduction potential of Y6 on the ability of OaPAC to convert ATP to cAMP. The formation of pyrophosphate (PPi) was monitored in both discontinuous and continuous formats using a coupled assay based on a PPi-dependent phosphofructokinase pyrophosphate reagent kit that results in the oxidation of NADH, which is monitored at 340 nm.[66,67] Using a discontinuous assay format in which the amount of PPi was quantified after the reaction was quenched by heating, only the 3-FY6 and 2,3-F_2Y6 variants had observable activity whereas 3,5-F_2Y6 and 2,3,5-F_3Y6 had no detectable activity. Fitting the data to the Michaelis-Menten equation provided k_{cat}/K_M values for 3-FY6 and 2,3-F_2Y6 OaPAC that were comparable with the wild-type. Finally, in contrast to the other variants, 2,3-F_2Y6 had residual activity in the absence of blue light, indicating that a population of this variant is in a pseudo-lit state which is able to convert ATP to cAMP in the absence of light.

The consumption of NADH as function of time was also monitored in a continuous assay format in which the coupled assay reagents were present during OaPAC photoactivation. Using this method, similar results were obtained for all the variants (**Figure 2.9, and Table 2.2**).

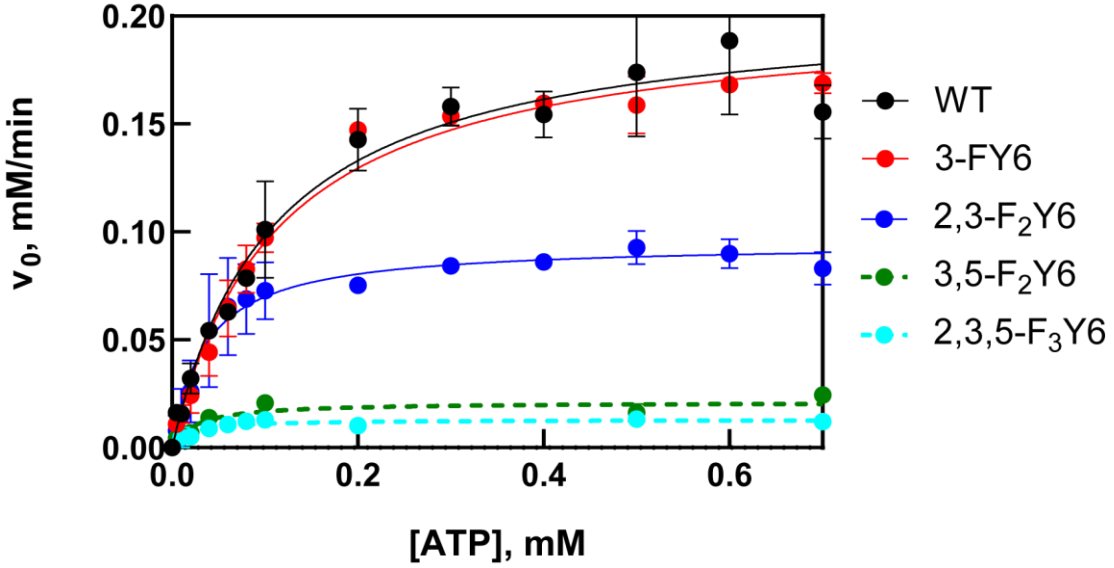

Figure 2.9. Michaelis-Menten plots of wild-type (WT) OaPAC and n-FY6 variants. Each point represents the initial velocity at each ATP concentration extracted from the linear portion of the A_{340} vs time plot under continuous illumination. The lines are the result of nonlinear fits to the Michaelis-Menten equation. Each data point is the average of 2 replicates where the error bars represent the standard error of the mean. (**The values plotted on y-axis here are absorbance values and have been later corrected to corresponding initial velocities calculated from absorbances, for the work reported in next chapter).

Table 2.2. Kinetic parameters for wild-type OaPAC and n-FY6 variants.

	pKa	k_{cat} (min^{-1})	K_M (mM)	k_{cat}/K_M (mM^{-1} min^{-1})
wild-type OaPAC	9.9	205 ± 11	0.12 ± 0.01	1888 ± 207
3F-Y6	8.4	202 ± 6	0.11 ± 0.01	1796 ± 182
2,3-F_2Y6	7.8	95 ± 5	0.04 ± 0.01	2664 ± 551
3,5-F_2Y6	7.2	***	***	***
2,3,5-F_3Y6	6.4	***	***	***

*** No Enzymatic activity detected.

Data were obtained under continuous illumination using 1 μM enzyme. (**The kinetic parameters here are based on the graph above and have been corrected in the next chapter)

Discussion:

Although the photochemistry of BLUF photoreceptors has been extensively studied using a variety of time-resolved approaches, these studies have been largely confined to BLUF domain proteins lacking the biologically-relevant output partner.[48,54,68-70] In the present work, we extend our analysis of the BLUF photocycle to OaPAC in which both the BLUF and adenylate cyclase output domains are contained in a single protein. Using TRIR and TRMPS, we investigated the OaPAC photoactivation mechanism, and compared it with other BLUF proteins. We further explored the impact of modulating the acidity of the conserved tyrosine Y6 on the light-controlled adenylate cyclase reaction. The photoactivation of the BLUF photoreceptors can be broadly distinguished based on the presence or absence of radical intermediates during light state formation. Whereas no radical intermediates can be observed during light-state formation in AppA, BlrB and BlsA, the photoactivation of PixD (Slr1694) and PapB involves PCET on the reaction pathway leading to the light state.[48,51,71,72] In the case of PixD, photoactivation of the flavin leads to a sequential formation of anionic ($FAD^{\bullet-}$) and neutral ($FADH^{\bullet}$) flavin radicals while in PapB a neutral flavin semiquinone FADH radical ($FADH^{\bullet}$) was observed as the intermediate before the formation of the signaling state.[54,71]

The TRIR and visible TA data indicate that two different processes can occur in the OaPAC photocycle after excitation. TRIR measurements on the wild-type protein and the Y6F mutant illustrate that if W90 is present, there is an electron transfer process from W90 to the flavin, forming the $FAD^{\bullet-}$–$TrpOH^{\bullet+}$ radical pair. TRIR and visible transient measurements on the wild-type and W90F mutant also indicate that after excitation a concerted proton-coupled electron transfer process occurs from the Y6 to the flavin, generating the $FADH^{\bullet}$–$Tyr^{\bullet}$ radical pair.

The role of proton transfer in the function of $OaPAC_{BLUF}$ was examined in a recent paper by the Zhong group where the authors replaced the tyrosine by a tryptophan (Y6W).[73] Kang et al.

observed a sequential electron transfer process: formation of the flavin anionic radical followed by the formation of the neutral semiquinone. The authors proposed that they observed proton rocking in which the tryptophan transiently donated a proton to the flavin to form the neutral semiquinone followed by a reverse proton transfer (PT); the rates of the forward and reverse PT were very close, being 51 ps and 52 ps, respectively. We have observed enhancement of the electron transfer process in other BLUF domain proteins (AppA, PixD) when the conserved tyrosine (Y21 and Y8, respectively) was replaced with a tryptophan, although this mutation resulted in the loss of protein activity. We expect a similar effect occurs in the case of the Y6W OaPAC mutant and plan to observe the effect of this mutation on the cAMP production.

The conserved tyrosine in BLUF domain proteins is essential for photoactivity and in every case, including OaPAC, replacement of this residue with phenylalanine results in a photoinactive protein. However, the precise role of the conserved tyrosine in the photoactivation mechanism depends on whether or not radical intermediates are present in the photocycle. In PixD, the 3000-fold increase in acidity of Y8 resulting from replacing Y8 with 2,3,5-F_3Y6 halts the photocycle at $FAD^{\bullet-}$ presumably because the tyrosine is ionized and can no longer function as the proton donor required for formation of $FADH^{\bullet}$. In contrast, replacement of Y21 in AppA has only a slight impact on the kinetics of light-state formation and every n-FY6 variant is photoactive. The biggest alteration in $AppA_{BLUF}$ was on the dark-state recovery where the change in Y21 pK_a led to a 4000-fold increase in the rate of dark-state recovery in H_2O while in PixD the change was only 15-fold.[54] The studies here show again that OaPAC photochemistry resembles PixD. For 3,5-F_2Y6 and 2,3,5-F_3Y6, the two variants with the most acidic phenol groups (pKa 7.2 and 6.4), no light state can be observed in either the absorption spectrum or the TRIR spectrum. In contrast for 3-FY6, where the phenol pKa is only 1.5 pH units more acidic than tyrosine, a 10 nm red shift is observed in the

flavin absorption spectrum upon excitation and the TRIR/TRMPS spectra are very similar to wild-type OaPAC. Finally, although a ~5 nm red shift in the flavin absorbance at 450 nm can be observed upon irradiation of 2,3-F_2Y6 OaPAC, no light-state transient at 1694 cm^{-1} can be observed in the TRIR and the photocycle apparently stalls at $FAD^{\bullet-}$. We speculate that the lack of observable light state in the TRIR data is because the yield of light state is low in this mutant given that this is a single shot experiment.

The presence of a covalently attached adenylate cyclase domain in OaPAC provides a unique opportunity to directly link the photochemistry of the BLUF domain with activation of the output domain. Using a coupled assay, light-dependent conversion of ATP to cAMP occurs with kcat, K_M and k_{cat}/K_M values of 205 ± 11 min^{-1}, 0.12 ± .01 mM and 1888 $mM^{-1}min^{-1}$, respectively. These values have not been previously reported for OaPAC, however Ohki et al. reported an ~20-fold change in enzymatic activity between dark and light states at a single ATP concentration.[16] In the pyrophosphate spectrophotometric assay, we observe a ~100-fold increase in activity for wild-type OaPAC upon photoexcitation. In agreement with time-resolved spectrosocopy, 3-FY6 OaPAC has adenylate cylase activity that is comparable to that of the wild-type protein, wherease 3,5-FY6 and 2,3,5-FY6 show no light-dependent catalytic activity. Interestingly, 2,3-F_2Y6 has similar k_{cat}/K_M value to wild-type OaPAC even though no light state can be observed in the TRIR spectrum and the steady state FTIR difference spectrum showed smaller light-induced changes in the protein modes in contrast to the wild-type. As noted above, a small red shift can be observed in the flavin absorption band at 450 nm, suggesting that light state can be formed when the protein is continously illuminated. We speculate that in the assay we are converting all the photoactive 2,3-FY6 into the light state whereas there is only a low yield of light state in the single-shot TRIR experiments (see above). Also, a population of 2,3-F_2Y6 variant is in a pseudo-lit state since in the

assay we observed coversion of ATP to cAMP in the absence of light. Therefore, in the case of the steady state IR difference measurement, the appearance of protein modes should appear suppressed compared to the wild type (see above).

Conclusion

Our time-resolved experiments on BLUF domain photoreceptors have been extended to OaPAC in which the BLUF domain is covalently attached to an adenylyl cyclase (AC) output domain. OaPAC is thus a good model system not only for studying photochemistry but also elucidating signal transduction between a BLUF domain and an output domain by monitoring the light-stimulated conversion of ATP to cAMP. Our work illustrates the direct impact of the photochemical processes in the BLUF domain on the output domain, which has not previously been shown in AppA, PixD or any other BLUF domain. Using ultrafast infrared and transient absorption spectroscopy we show that the photoactivation mechanism of OaPAC involves concerted proton electron transfer from the conserved Y6 to the excited state of FAD (FAD*). This mechanism is slightly different from the one observed in PixD, where the photoactivation mechanism involves a sequential proton-coupled electron transfer from Y8 to FAD*. Instead, in the case of OaPAC protonation of the flavin occurs together with the electron transfer step from Y6 to the flavin. The role of Y6 in the photocycle of OaPAC was probed via unnatural amino acid mutagenesis. Replacement of Y6 with n-FY analogues increases the acidity of the phenol hydroxyl group and reduces the rate of electron transfer. Specifically, altering the pK_a and/or reduction potential of the flavin had a profound impact on light-state formation for 2,3-F_2Y6, 3,5-F_2Y6 and 2,3,5-F_3Y6 where the photocycle is halted at $FAD^{\bullet-}$. Using an enzyme assay that couples PPi production to consumption of NADH, we quantified the adenylate cyclase activity of wild-type OaPAC and also of the n-FY6 variants to interrogate the impact of the Y6 pKa on the light-

activated conversion of ATP to cAMP and PPi. Only the n-FY6 variants with pKa values of 7.8 or higher were able to catalyze cAMP formation, while variants with lower pKa values were inactive since the photocycle was halted at $FAD^{\bullet -}$. While the 2,3-F_2Y6 OaPAC variant (pKa 7.8) had light-dependent adenylate cyclase activity, no light state was observed in the TRIR which we propose is due to the low yield of product formation given the single-shot format of the experiment. Collectively, the results shed new light on the photoactivation mechanism of BLUF domain photoreceptors.

Chapter 3

This chapter has been accepted for publication in *ACS Chemical Biology*.

Chapter 3: Probing the signaling transduction mechanism of the light-activated adenylate cyclase OaPAC using unnatural amino acid mutagenesis

Samruddhi S. Jewlikar,[†] Jinnette Tolentino Collado,[†] Madeeha I. Ali,[†] Aya Sabbah,[†] YongLe He,[†] James N. Iuliano,[†] Christopher R. Hall,[‡] Katrin Adamczyk,[‡] Gregory M. Greetham,[‖] Andras Lukacs,[§,*] Stephen R. Meech,[‡,*] and Peter J. Tonge[†,‡,*]

[†]*Department of Chemistry, Stony Brook University, Stony Brook, NY, 11794-3400, United States;*

[‡]*School of Chemistry, University of East Anglia, Norwich, NR4 7TJ, United Kingdom;*

[§]*Department of Biophysics, Medical School, University of Pecs, Szigeti ut 12, 7624 Pecs, Hungary;*

[‖]*Central Laser Facility, Research Complex at Harwell, Rutherford Appleton Laboratory, Didcot, OX11 0QX, United Kingdom*

Author Contributions:

SJ: Conception and experimental design

SJ, JTC, MIA: Samples preparation and handling

SJ, JTC, MIA, AS, JNI, CRH, KA: Data collection

SJ, JTC, YH: Data analysis and interpretation

PJT, SJ: Drafting the article, critical revision of the article

PJT, SJ: Final approval of the version to be published

GMG: Central Laser Facility (CLF) Scientists

Introduction:

Optogenetics combines optical and genetic approaches to control cellular events using light.[74] Central to this technology are photoactive proteins that are fused to effector domains to enable the light-dependent control of processes such as enzyme activity, gene expression, and signaling. The rational design and optimization of new optogenetic devices requires a detailed understanding of the photoactivation mechanism of naturally occurring photoreceptors, in particular those in which both the light absorbing and effector domains are part of the same protein. Flavin-dependent photoreceptors, including those that contain blue-light using FAD (BLUF) or light oxygen voltage (LOV) domains, are popular choices for the creation of novel optogenetic tools,[75,76] and a key goal is to determine how ultrafast excitation of the flavin chromophore results in formation of the light-activated state on the μs-s time scale.[77,78]

BLUF domain photoreceptors are found in bacteria and unicellular eukaryotes,[79] where light activated signaling is accomplished either through non-covalent or covalent interaction with downstream effector output partners. BLUF photoreceptors control a diverse array of physiological processes including photosystem biogenesis (AppA),[80] phototaxis (PixD/Slr1694),[81] and virulence (BlsA).[82] In addition, BLUF domain photoreceptors have been discovered that regulate the production of the important signaling molecule cAMP in response to blue light, including PACα and PACβ from *Euglena gracilis*,[83] bPAC from *Beggiatoa*,[84] and OaPAC from *Oscillatoria acuminata*.[85]

OaPAC is a 366 residue homodimer containing an N-terminal BLUF domain and a C-terminal class III adenylate cyclase (AC) domain (**Figure 3.1**).[85] The two monomers interact in a head to head configuration with each BLUF domain providing a helix to a coiled coil that connects the BLUF domain with the AC domain. Similar to other BLUF photoreceptors, the BLUF domain is comprised of a ferredoxin-like fold in which the isoalloxazine ring of the flavin is surrounded

by two α-helices and a five-stranded β-sheet.[86] In addition, several conserved residues form a hydrogen bond network that interacts with the isoalloxazine ring including Y6, Q48 and N30.[79] Light absorption results in a ~10 nm red shift in the spectrum of the oxidized isoalloxazine chromophore which is caused by rotation of Q48, possibly preceded by keto-enol tautomerism,[87] so that a second hydrogen bond is formed with the flavin C4=O group (**Figure 3.1**).[88-91]

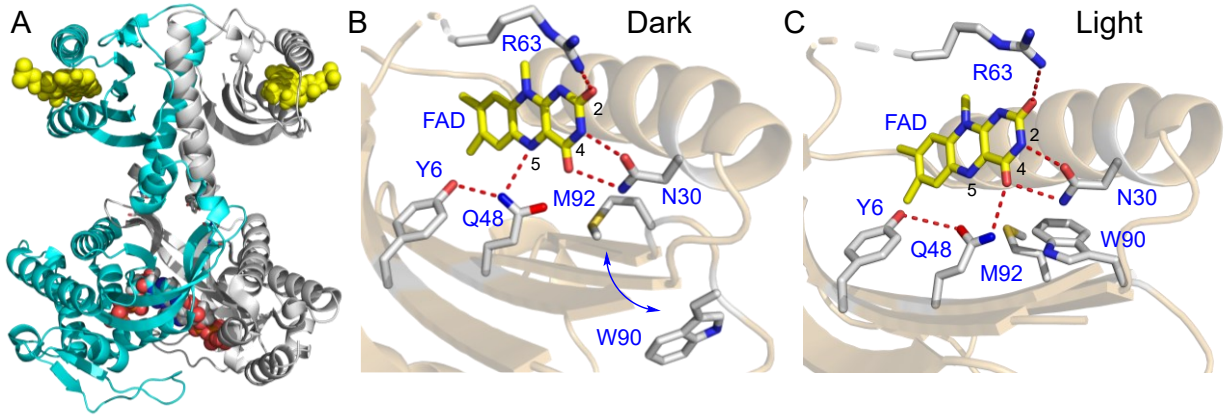

Figure 3.1: The OaPAC dimer and flavin binding pocket. A) The OaPAC dimer (PDB: 8QFE). FAD and ATP are shown as spheres in the BLUF and AC domains, respectively. B) and C) Proposed structural changes in the flavin binding pocket upon photoactivation based on the structures of OaPAC determined by time-resolved crystallography (PDB: 8QFE and 8GFG).[92] The figure was made using pymol.[93]

While some of the light-stimulated changes in the BLUF photoreceptors are well understood, outstanding mechanistic issues include the role of electron transfer in photoactivation, and the position of a semi-conserved Trp (W90) and conserved Met (M92) which may communicate changes in the hydrogen bond network to the protein matrix.[94-97] For the wild type OaPAC, excitation of FAD leads to a concerted proton-coupled electron transfer (PCET) and the formation of the neutral flavin radical (FADH$^{\bullet}$) which reacts with Y$^{\bullet}$ radical to form the final light state where the flavin is in oxidized form.[98] In addition, the structural dynamics that drive output domain activation also remain to be fully elucidated. To address one of these questions, we previously

replaced Y6, the conserved Tyr in OaPAC, with fluoro-Tyr residues to increase the acidity of the phenolic hydroxyl group. While the 3F-Y6 and 2,3-F_2Y6 variants underwent the complete photocycle and catalyzed the conversion of ATP into cAMP, activity was abolished in the 3,5-F_2Y6 and 2,3,5-F_3Y6 variants where the photocycle was halted at $FAD^{\bullet-}$, demonstrating that proton transfer plays an essential role in initiating the structural reorganization of the AC domain.[98] We also previously studied the roles of the conserved Gln, Q48, as well as D67 in photoactivation. These studies demonstrated that the Q48E mutation alters the primary electron transfer process and switches the enzyme to a permanently 'on' state,[99] whereas replacing D67 with Asn accelerated the primary electron transfer process.[100] In the present work, we are exploring the signal transduction at a more remote location from flavin by studying Y125.

Most BLUF proteins including OaPAC contain a Trp that is located near the flavin binding site (W90 in OaPAC). Structural studies of multiple BLUF proteins together with biophysical experiments and site-directed mutagenesis support a key role for the Trp in photoactivation. In particular, it has been proposed that the indole side chain rotates between Trp_{in} and Trp_{out} conformations accompanied possibly by relocation of the conserved Met (M92 in OaPAC). Using cryo-trapping, Chretien et al have obtained support for this model and propose that W90 moves from a Trp_{out} to a Trp_{in} conformation during light state formation that is accompanied by movement of M92 out of the pocket (**Figure 3.1**).[92] However, this model contrasts with earlier structural data on OaPAC in which the Trp undergoes only a relatively small movement and is found in a Trp_{out} conformation in both dark and light states.[85,101]

In the present work, we employed site-directed and unnatural amino acid mutagenesis coupled with time-resolved and steady-state FT-IR spectroscopy as well as kinetic assays to probe the local structural changes in OaPAC and map the signal transduction pathway in solution.

Following similar studies on the BLUF proteins AppA and PixD,[102] we replaced W90 with the infrared (IR) probe azido-Phe (AzPhe). We also introduced AzPhe into two other positions in OaPAC at F103 and F180. F103 is on a loop between β-sheet 5 and α-helix 3, which undergoes a significant structural rearrangement on photoactivation,[85] whereas F180 is in the central core of the AC domain (**Figure 3.2**). Finally, we analyzed the importance of Y125, which is located at the junction between the α-3 helix and the AC domain and interacts across the dimer interface with N256, by replacing this residue with fluoro-Tyr residues. Key findings based on the spectroscopic and kinetic characterization of the substituted OaPAC proteins includes support for the movement of W90 from a Trp_{out} to a Trp_{in} conformation during light state formation and that signal transduction requires Y125 to be protonated. Collectively the data provide further insight into the mechanism of signal transduction in OaPAC.

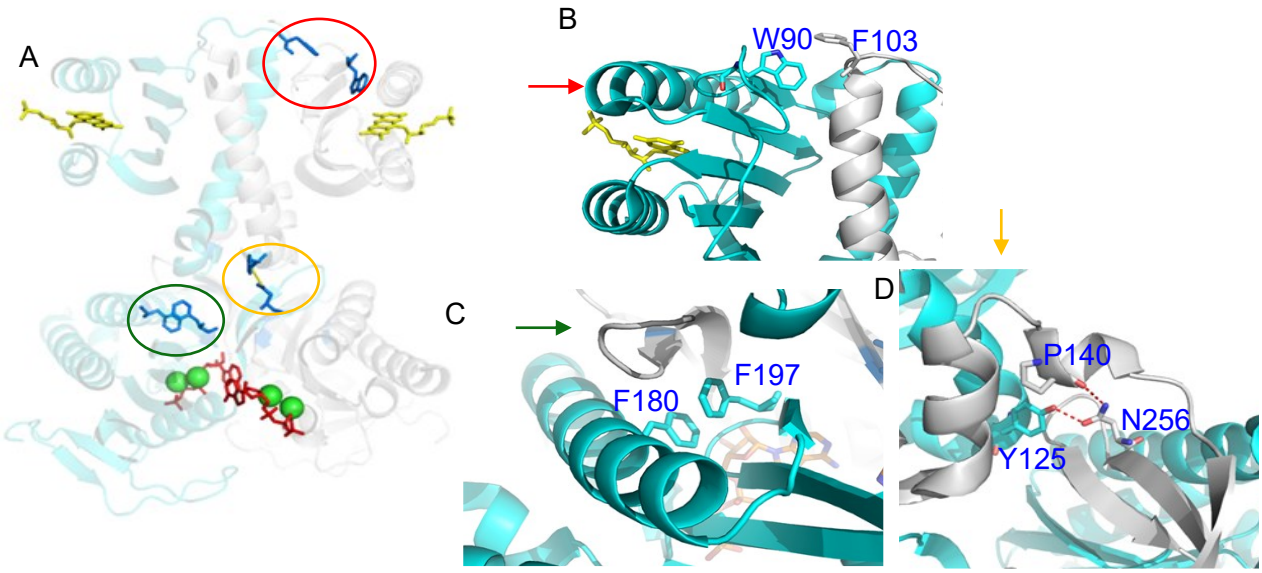

Figure 3.2: Residues replaced with unnatural amino acids. A) OaPAC dimer with depicting the regions of chosen mutation sites B) W90 and F103 were replaced with AzF. These residues interact across the dimer interface at the tip of the central helix. C) F180 was replaced by AzPhe. D) Y125 was replaced by fluoro-Tyr analogs. The figure was made using pymol,[20] from PDB:8QFE.[19]

Methods:

Tyrosine phenol lyase expression and purification

BL21(DE3) pLysS cells were transformed with the pET23b C-terminal His-TPL plasmid and a single colony was used to inoculate 10 mL of LB media supplemented with 100 µg/mL ampicillin (Amp) and 30 µg/mL chloramphenicol (Cam). After incubating at 37 °C in a shaker (250 rpm), the culture was used to inoculate 1 L of 2x-YT media in a 4 L flask, also supplemented with Amp/Cam. The culture was incubated at 37 °C until the OD600 reached ~0.8, and then the temperature was lowered to 25 °C for 30 min followed by the addition of 1 mM IPTG to induce protein expression. After overnight incubation, the cells were harvested through centrifugation at 5500 rpm (4 °C), and the resulting cell pellet was stored at -20 °C. After thawing, the cell pellet was resuspended in lysis buffer (0.1 M NaH_2PO_4 buffer pH 7.0 containing 150 mM NaCl, 5 mM imidazole, 5 mM β-mercaptoethanol, and 0.1 mM pyridoxal-5'-phosphate), and the cells were lysed via sonication (6 cycles of 30 s at 18 W with 5 min intervals on ice between cycles). Removal of cell debris was achieved by centrifugation at 40,000 rpm for 1 h, and subsequent purification of TPL was carried out utilizing Ni-NTA chromatography. The column was washed with 0.1 M NaH_2PO_4 buffer pH 7.0 containing 150 mM NaCl, and 5 mM β-mercaptoethanol, supplemented with increasing concentrations of imidazole (0, 5, 10, and 20 mM), after which TPL was eluted using the same buffer containing 250 mM imidazole. Fractions containing TPL were pooled, and imidazole was removed by buffer exchange with 0.1 M NaH_2PO_4 buffer pH 7.0 containing 150 mM NaCl using ultracentrifuge tubes.

Fluoro-Tyr synthesis using tyrosine phenol lyase

Each fluoro-Tyr was synthesized from respective fluorophenol in a reaction mixture comprised of 10 mM fluorophenol, 60 mM pyruvic acid, 40 μM pyridoxal-5'-phosphate, 30 mM ammonium acetate, and 5 mM β-mercaptoethanol that was adjusted to pH 8.0 using NH_4OH.[98,115,116] Subsequently, 160 units/L (0.53 mg =1 unit) of purified TPL was added followed by incubation in the dark for 4 days at RT. During the incubation, 30 units of TPL was added daily. TPL was then precipitated by acidification of the reaction mixture using 5% trichloroacetic acid, and then removed by centrifugation at 5,000 rpm (4 °C) and gravity filtration. The supernatant was extracted twice with ethyl acetate to remove excess phenol, and the aqueous layer was then loaded onto an activated cation exchange Amberlite column, prepped with 200 mL of 2 N HCl and washed with deionized water to eliminate excess HCl. The column was then washed with deionized water and 250 mL of 10% NH_4OH was used to elute the fluoro-Tyr. Fractions (10 mL) containing fluoro-Tyr were identified using ninhydrin stain (4% ninhydrin), combined, concentrated using a rotary evaporator, lyophilized. The mass spectra, ^{1}H NMR, and ^{19}F NMR spectra matched that reported by us previously.[98]

Fluoro-Tyr incorporation using orthogonal aminoacyl-tRNA-synthetases

Incorporation of the fluoro-Tyr analogues utilized the E3 orthogonal polyspecific aminoacyl-tRNA synthetase encoded on a pEVOL plasmid and an expression vector for OaPAC with a C-terminal His tag in which the codon for Y125 had been mutated to TAG. The pCOLD C-terminal His-OaPAC-Y125TAG plasmid was co-transformed with the E3 pEVOL plasmid into BL21 (AI) cells, and a single colony was utilized to inoculate a 10 mL culture of 2x-YT media, supplemented with 100 μg/mL of ampicillin and 30 μg/mL of chloramphenicol. The culture was

incubated overnight at 37 °C on a shaker at 250 rpm, after which 5 mL was used to inoculate 500 mL of 2x-YT media containing 100 μg/mL of ampicillin and 30 μg/mL of chloramphenicol, in a 4 L flask. The culture was incubated at 37 °C in a shaker (250 rpm) until the OD600 reached ~0.3. Subsequently, 0.05% of L-arabinose was added to the media to induce expression of the E3 aminoacyl-tRNA synthetase. After 1 h, a fluoro-Tyr analogue dissolved in NaOH, was added to the media to a final concentration of 1 mM. The OD600 was continuously monitored, and when it reached ~0.8-1, the temperature was lowered to 18 °C, and 1 mM IPTG was added to the media. Following an overnight incubation at 18 °C in a shaker (250 rpm), the cells were harvested via centrifugation at 5,500 rpm for 20 min, and the resulting cell pellet was stored at -20 °C prior.

For protein purification, the cell pellet from the 1 L culture was resuspended in 40 mL of lysis buffer (50 mM NaH_2PO_4 pH 8.0, 350 mM NaCl) together with protease inhibitor (PMSF, 250 μM final concentration), β-mercaptoethanol (14 μL), and FAD (10 mg), and the cells were then lysed using sonication. Subsequently, the cell lysate was centrifuged at 40,000 rpm for 1 h at 4 °C to remove cell debris. The supernatant was loaded onto a Ni-NTA column equilibrated with lysis buffer which was then washed with lysis buffer containing increasing concentrations of imidazole (5 mM, 10 mM, and 20 mM). The OaPAC protein was eluted using lysis buffer containing 250 mM imidazole. Fractions containing OaPAC were pooled, and the imidazole was removed using A HiPrep 26/10 desalting column with 20 mM Tris pH 8.0 buffer containing 150 mM NaCl. After filtering through a 0.22 μm PVDF membrane, the protein purity was confirmed by SDS-PAGE and the concentration was determined using a UV-Visible spectrophotometer. The fluoro-Tyr incorporation was assessed by mass spectrometry.

Incorporation of azido-Phe (AzPhe)

Incorporation of AzPhe was performed using the pDule aminoacyl tRNA synthetase (pDuleCNPhe). The method used followed that described above except that the pCOLD C His-OaPAC-plasmid containing the TAG mutation at the appropriate position was co-transformed with the pDule plasmid and selection was performed using with 100 μg/mL ampicillin and 50 μg/mL spectinomycin. L-arabinose (0.05% w/v) was used to induce expression of the pDule synthetase and after 1 h 110 mg of 4-azido-L-Phe was added as a powder to achieve a final concentration of 1 mM in 2x-YT media. Subsequent purification of the Az-Phe-substituted OaPAC proteins was performed as described above and incorporation of the unnatural amino acid was assessed by mass spectrometry. The protein was concentrated to 2-2.5 mM in 20 mM Tris buffer pH 8.0 containing 150 mM NaCl for IR spectroscopy. For experiments in D_2O the protein was exchanged into the same buffer prepared using D_2O (pD 8.0).

Steady-state FTIR spectroscopy

Steady-state FTIR spectra were obtained on a Vertex 80v (Bruker) FTIR spectrometer with 3 cm^{-1} resolution. The protein sample (50 μL, 2.5 mM in buffer) was placed between two CaF_2 windows with a 6 μm spacer in a Harrick cell and 256 scans were acquired. The light state was then generated by illuminating the sample continuously using a 455 nm LED (Prizmatix, Ltd.) placed into the sample compartment and focused onto the cell. The dark state spectrum was subtracted from the light state spectrum to generate the light minus dark (L-D) difference spectrum. The dark and light steady state spectra were obtained by subtracting the spectrum of the buffer measured with the same parameters as protein samples. All measurements were performed at RT. We used 450 nm LED to irradiate the samples and the spectrum of AzPhe before irradiation and after several rounds of irradiation were compared to ensure that there is no photodegradation of

Azido on blue light irradiation. The azido group has absorption maxima at around 270 nm in the UV-Visible range.

Time Resolved Multiple Probe Spectroscopy (TRMPS)

TRMPS spectra were obtained at 20 °C from 100 fs to 1 ms at the STFC Central Laser Facility. The TRMPS method has been described, and previously used by us to analyse the photochemistry and site-specific protein dynamics of BLUF proteins.[98,117,118] Light sensitive samples were analysed using a rastered flow cell to minimize photochemistry and data were acquired using a 450 nm pump operated at 0.6-0.8 μJ per pulse and a repetition rate of 1 kHz. The spectral resolution was 3 cm^{-1} and the temporal resolution was 200 fs. For the AzPhe measurement in the region of 2050-2200 cm^{-1}, the W90AzPhe protein was concentrated to ~ 2 mM in H_2O buffer (20mM Tris, 150 mM NaCl, pH 8.0). For the fingerprint region, the sample was buffer exchanged to D_2O buffer (20mM Tris, 150 mM NaCl, pD 8.0) and concentrated to ~ 0.8 mM. After the measurements were recorded, the extent of photoconversion was shown to be negligible using absorbance spectroscopy. Spectra were calibrated relative to the IR transmission of a pure *cis* stilbene standard sample placed at the sample position. Data were analysed globally using the sequential model with Glotaran.

Adenylate cyclase activity assay

The adenylate cyclase activity of OaPAC performed using an Ocean Optics spectrophotometer equipped with a 12.5 mm width, 10 mm path length quartz cuvette. Assays contained OaPAC (1 μM), ATP (10 μM to 800 μM) and the master mix of reagents which contained inorganic pyrophosphatase, purine nucleoside phosphorylase, 20X buffer (1 M Tris-HCl, 20 mM $MgCl_2$, pH 7.5) and dH_2O as diluent. In this coupled assay, the PPi produced from the conversion of ATP to cAMP is converted to two equivalents of Pi by inorganic pyrophosphatase and the Pi is then

quantified following reaction with MESG/PNP and detection at 360 nm. The reaction mixture was incubated in the cuvette in the dark and absorbance at 360 nm was monitored for 40 s. The cuvette was then continuously illuminated with blue-light and absorbance was monitored at 360 nm to determine initial velocities.

Results:

AzPhe as an IR probe of local structural dynamics

AzPhe has previously been used to explore the structural changes experienced by specific residues in the BLUF proteins AppA and PixD caused by photoactivation,[102] and in other photoreceptors such as Channelrhodopsin,[103] and bacteriophytochrome.[104] To extend these studies to the present system, we identified three positions in OaPAC based on their location in the protein: W90 which is proposed to play a pivotal role in photoactivation, F103 which is present on the loop between β-sheet 5 and α-helix 3 and interacts with the 'out' conformation of W90 across the dimer interface, and F180 which is in the core of the AC domain.

W90AzPhe, F103AzPhe and F180AzPhe OaPAC were expressed using 21st pair methodology,[105] using an OaPAC construct with a C-terminal His-tag. Following purification with Ni-affinity chromatography, the UV-visible absorption spectrum and rate of dark state recovery was determined for each protein. Similar to wild-type OaPAC, each AzPhe-substituted protein underwent the characteristic red shift in the flavin absorption spectrum and recovered to the dark state with τ~5s with the exception of W90AzPhe which recovered ~5-fold more slowly (τ~28s) (**Table 3.1**).

Table 3.1: Absorbance Maxima and Catalytic Activity of the OaPAC Variants

OaPAC	Dark λ_{max} (nm)	Light λ_{max} (nm)	τ_{rec}[1] (s)	k_{cat} (min^{-1})	K_m (μM)	k_{cat}/K_m[2] (μM^{-1} min^{-1})
Wild-type	445	457	4	11.8±1.1	65±20	0.18±0.05
F103AzPhe	444	455	4	8.8±0.2	102±7	0.09±0.02
W90AzPhe	444	456	28	12.3±0.4	103±12	0.12±0.03
F180AzPhe	444	456	5	NA[3]	NA[3]	NA[3]

3F-Y125	443	457	9	9.4±1.4	86±38	0.11±0.04
3,5-F_2Y125	443	456	6	NA[3]	NA[3]	NA[3]
2,3,5-F_3Y125	444	454	4	NA[3]	NA[3]	NA[3]
N256A	444	457	7	NA[3]	NA[3]	NA[3]
N256Q	445	458	4	NA[3]	NA[3]	NA[3]
N256D	444	451	7	NA[3]	NA[3]	NA[3]

[1]The rate of dark state recovery was monitored at 443 nm.

[2]Catalytic activity was determined by quantifying the rate of PPi formation following irradiation at 450 nm. Errors are the standard deviation from two or more biological replicates.

[3]NA, no detectable activity.

We have previously estimated the dark state activity of wild type OaPAC and we observed a 100-fold change in the activity for wild type OaPAC upon photoexcitation.[98] The dark and light state activity of each protein was assessed using a discontinuous assay that monitored the time-dependent formation of inorganic pyrophosphate (PPi) (**Table 3.1**). Whereas W90AzPhe, and F103AzPhe had activity in the light state similar to the wild-type enzyme, F180AzPhe OaPAC had no detectable activity (**Table 3.1**).

Steady-state difference FTIR spectra of Az-Phe mutants

We then obtained light-minus dark steady state FTIR spectra of W90AzPhe, F103AzPhe and F180AzPhe OaPAC (**Figure 3.3**). The azido stretching vibration of W90AzPhe demonstrated a significant perturbation between the light and dark states whereas only a minor perturbation was observed for F103AzPhe, revealing that the environment of the AzPhe residue at position 103 is similar in the two states of the protein. In addition, no change was observed in the environment of

F180AzPhe, consistent with the observation that this mutation leads to a catalytically inactive enzyme.

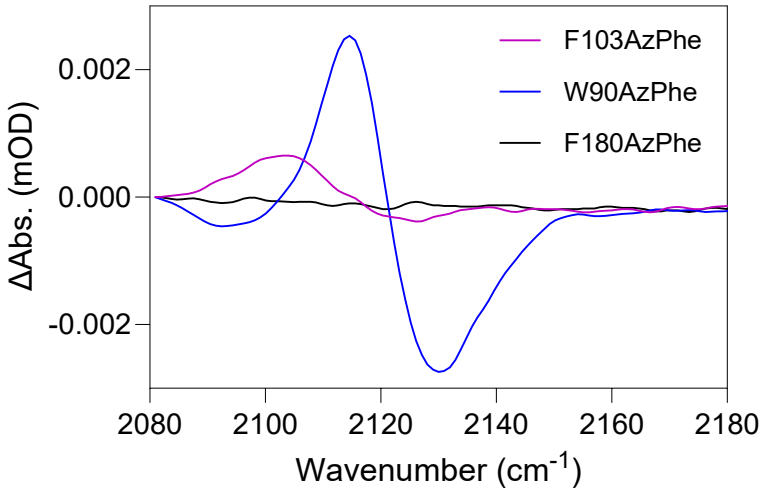

Figure 3.3: Difference infrared spectra of the AzPhe OaPAC variants. Light minus dark steady state infrared spectra of W90AzPhe (blue), F103AzPhe (purple) and F180AzPhe (black). The difference spectra were acquired by subtracting the FTIR spectrum of the sample obtained before irradiation from that obtained during continuous 450 nm irradiation.

TRMPS and TRIR of OaPAC variant W90AzPhe

To provide further information on the environmental changes experienced by W90AzPhe, we used ultrafast IR to monitor the difference spectrum of the azido stretch as a function of time following light absorption (**Figure 3.4**). The temporal evolution of the AzPhe at W90 position shows a negative bleach at 2128 cm^{-1} within ~ 1 ns and deepens on the µs timescale as a transient at 2111 cm^{-1} evolves. **Figure 3.4B** shows the evolution-associated difference spectra (EADS) which represents the spectral evolution over time. To generate the EADS, time-resolved data (**Figure 3.4A**) were globally analyzed in Glotaran using a sequential decay model of four components in which the lifetime of three components were allowed to vary, while the fourth component was kept constant (indicating a product with effectively infinite lifetime), yielding

three-time constants of 1.3 ns, 3.03 µs, and 150 µs. The final spectrum of the W90AzPhe evolves on the µs timescale and is similar to the steady state IR difference spectrum. Unlike the TRIR of W104AzPhe AppA$_{BLUF}$ and W91AzPhe PixD,[102] no evolution of the IR spectrum of W90AzPhe OaPAC is detected on the ps timescale. The instantaneous response of the W104AzPhe in AppA and W91AzPhe in PixD was taken as evidence for communication of the AzPhe with the hydrogen bond network surrounding the flavin, i.e. a Trp$_{in}$ conformation, and the absence of an instantaneous perturbation in the spectrum of W90AzPhe is thus consistent with a Trp$_{out}$ conformation in OaPAC.

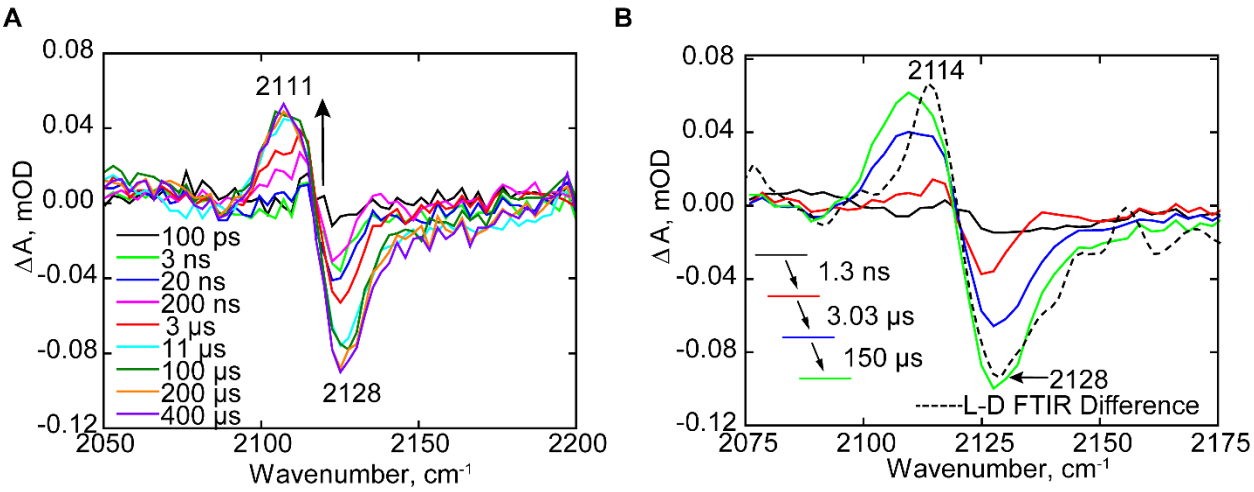

Figure 3.4: TRMPS spectra of the W90AzPhe OaPAC dark state. A) Time resolved IR difference response of the azido mode following ultrafast excitation of isoalloxazine cofactor in OaPAC at the W90 position. B) EADS of W90AzPhe obtained from globally fitting the time-resolved data in A to a sequential first order kinetics model with an initial state (black) two intermediate states (red, blue) which form on a ns-µs timescale, and subsequently relaxes to a final state (green). The final state is compared with the FTIR difference spectra (black dash line). All analyses used the Glotaran software package.

We also measured the time-resolved IR spectra of W90AzPhe OaPAC in the fingerprint region to correlate the protein structural changes to the dynamics observed in the azido region (**Figure 3.5**). The EADS, generated by a global fit of the data using two time constants of 1.1 ns

and 146 µs, shows that key intermediate states form within the first 3 ns that are detected in both the fingerprint and azido stretch regions of the spectrum and likely represent changes to the chromophore and proximal protein matrix. Comparison to the data obtained for wild-type OaPAC,[98] indicates that the AzPhe substitution has not affected the overall photocycle and the structural change to the rest of the protein accompanying light activation. For instance, the 1530 cm^{-1} indicates formation of $FADH^{\bullet}$, and thus that PCET has not been affected while the 1692 (+)/11704 (-) cm^{-1} transient can be assigned to a red shift of the flavin C4=O mode due to the additional hydrogen bond formed between the C4=O and Q48 in the light state of OaPAC. The subsequent slower changes on the µs timescale, such as the transients at 1640 (+)/1620 (-) cm^{-1} assigned to protein secondary structure, correlate with evolution of the AzPhe and result from formation of the final signaling state of the protein.

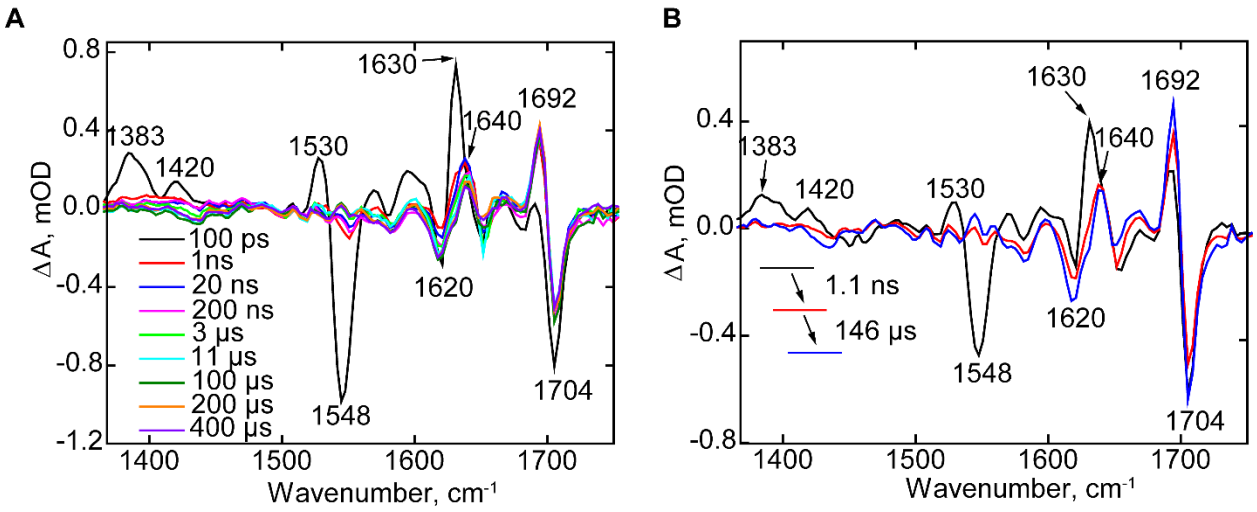

Figure 3.5. TRMPS of W90AzPhe OaPAC dark state. (A) Temporal evolution of the W90AzPhe OaPAC spectra recorded between 100 fs and 1ms after 450 nm excitation. (B) EADS of W90AzPhe OaPAC obtained from a global fit of the data in A.

The intersubunit hydrogen bond between Y125 and N256

Y125 is a fully conserved residue across all photoactivated adenylate cyclase enzymes and is present at the interface between the α3 helix and AC domain where it forms an intersubunit hydrogen bond with N256. Replacement of Y125 with Phe results in a catalytically inactive protein,[85] a result also observed in the related photoreceptor bPAC.[106] To provide more information on the role of this key hydrogen-bonding interaction in transducing the signal from the BLUF to the AC domain, we modulated the acidity of the Y125 hydroxyl group by replacing Y125 (pKa 9.9) with 3-fluoro-Tyr (3-FY, pKa 8.4), 3,5-difluoro-Tyr (3,5-F_2Y, pKa 7.2) and 2,3,5-trifluoro-Tyr (2,3,5-F_3Y, pKa 6.4). We also replaced N256 with Ala, Asp, and Gln residues.

The fluoro-Tyr variants were prepared as described in the methods section, and the UV-visible absorption spectrum and rate of dark state recovery was determined for each protein. As observed for the AzPhe variants, the 443 nm FAD absorption band for each fluoro-Tyr protein red shifted by ~12 nm upon illumination and recovered to the dark state with τ~4-9s (**Table 3.1**). We then analyzed the catalytic activity of each variant and found that the 3F-Y125 OaPAC retained light-activated adenylate cyclase activity, while replacing Y125 with 3,5-difluoro-Tyr and 2,3,5-trifluoro-Tyr resulted in loss of activity in the light state. Michaelis-Menten parameters for 3F-Y125 OaPAC were similar to those for the wild-type enzyme (**Table 3.1**).

Given the effect of lowering the Y125 pKa on catalytic activity we attempted to determine the pH dependence of the wild-type enzyme. However, whereas OaPAC had similar activity at pH 8-9, no activity was observed at pH 7.0 and 7.5, preventing the pH dependence from being determined. The loss of activity resulting from a relatively small change in pH may reflect a pH induced structural change of the protein rather than the change in ionization state of a single residue. We also replaced N256 with Ala, Asp, and Gln residues. Although each N256 mutant

retained the light-induced red shift in FAD absorbance that recovered to the dark state on a similar time scale to that of wild-type OaPAC (τ 4-7s), none of these OaPAC mutants had detectable catalytic activity (**Table 3.1**), again supporting the importance of the Y125-N256 hydrogen bond in formation of the OaPAC light state.

Discussion:

OaPAC is a light-activated adenylate cyclase in which both the photosensing and catalytic domains are part of the same protein. As a consequence, OaPAC is a model for elucidating the mechanism of signal transduction in BLUF photoreceptors, information that is critical to the design and optimization of novel optogenetic devices. In the present work, we have used unnatural amino acid mutagenesis to evaluate key sites thought to be critical for photoactivation including W90, which lies close to the chromophore, F103 which is present on the loop between β-sheet 5 and α-helix 3 and interacts with W90 across the dimer interface, F180 which is in the adenylate cyclase domain, and Y125 which forms an intersubunit hydrogen bond with N256 in the OaPAC dimer.

The IR probe AzPhe was used to replace W90, F103 and F180. All three OaPAC variants retained the characteristic red shift in FAD absorbance upon illumination and recovered to the dark state with similar rates as the wild-type although W90AzPhe OaPAC recovered ~5-fold more slowly (**Table 3.1**). It was subsequently found that F180AzPhe was catalytically inactive, and in keeping with this observation, the steady-state light minus dark FTIR difference spectra of AzPhe180 OaPAC indicated that there was no change in the environment of the AzPhe group upon photoexcitation (**Figure 3.3**). Therefore, the F180AzPhe mutation prevents activation of the adenylate cyclase domain and is locked in the dark state, although the protein environment around the flavin responds to light absorption. Analysis of the X-ray structure of OaPAC shows that F180 forms a **π-π** stacking interaction with F197, and previous studies have shown that the F197S mutation is catalytically inactive supporting the functional importance of the F180-F197 interaction.[85]

In contrast, to F180AzPhe OaPAC, both the W90AzPhe and F103AzPhe OaPAC variants had similar catalytic activity in the light state compared to wild-type OaPAC (**Table 3.1**). FTIR

difference spectra of these variants indicated a red-shift in the azido mode upon photoexcitation, however the intensity of the difference spectrum for F103AzPhe OaPAC is significantly smaller than that for W90AzPhe OaPAC. F103 is located on the loop between β-sheet 5 and α-helix 3 which undergoes a significant structural rearrangement on photoactivation.[92] However the low intensity of the F103AzPhe IR difference spectrum suggests that the AzPhe group experiences a similar environment in both the dark and lights states. Thus, either the azido group in F103AzPhe does not interact with W90 in the dark state, or W90 occupies similar positions in the dark and light states.

Many BLUF domain photoreceptors contain a Trp that is located close to the flavin binding pocket including OaPAC (W90). This includes the BLUF proteins AppA and PixD (Srl1694) where structural data revealed that the conserved Trp (W104 in AppA and W91 in PixD) can adopt a conformation in which the indole side chain is close to the flavin binding pocket (Trp_{in}) or has rotated out of the pocket (Trp_{out}).[86,91,107] Replacement of W104 with Ala in AppA decouples the light-induced changes in the flavin binding pocket from protein structural changes, and this observation together with other structural, biochemical, biophysical and computational studies, indicates that the Trp is directly involved in signal transduction, leading to the proposal that movement of the Trp is linked to formation of the light activated state. [87,108-111] A Met residue is also located close to the Trp (M106 in AppA and M93 in PixD), resulting in proposed models in which the Trp and Met side chains exchange positions during photoactivation. To determine the dynamics of the Trp and Met residues in AppA and PixD, we replaced each residue with AzPhe and used TRIR to analyze the time-dependent evolution of the azido IR spectrum. Although AzPhe substituted for M106 and M93 responded only weakly to excitation, the azido spectrum of AzPhe at positions 104 and 91 responded instantaneously and then showed complex evolution on the sub-

ns timescale leading to the conclusion that the AzPhe occupies an "in" configuration, in both $AppA_{BLUF}$ and PixD, consistent with solution NMR studies.[112,113]

Site-directed mutagenesis also supports a critical mechanistic role for W90 in OaPAC,[41] and X-ray structural studies have shown that W90 occupies a Trp_{out} conformation in the dark state.[85,92,101] Although the initial 'light-state' structure of OaPAC showed only a small perturbation in the position of W90,[85,101] the recent time-resolved X-ray structural studies on OaPAC provide support for the movement of W90 from a Trp_{out} to a Trp_{in} conformation and relocation of M92 away from the flavin.[92] In addition, ^{19}F NMR experiments suggest that W90 can occupy multiple positions ($W_{in}NH_{in}$, $W_{in}NH_{out}$ and W_{out}) and that the prevalence of Trp_{out} conformations observed in the X-ray structures of BLUF proteins may be the result of crystal packing.[113] Thus, to provide further insight into the structural dynamics of W90, we used TRIR in addition to steady state FTIR to analyze time-dependent changes in the IR spectrum of W90AzPhe OaPAC. Both the W90AzPhe azido stretch at ~2100 cm^{-1} and the fingerprint region respond on similar time constants to photoexcitation (1.3 ns, 3.03 μs and 150 μs compared to 1.1 ns and 140 μs) indicating that incorporation of AzPhe has not decoupled excitation of the flavin from activation of the adenylate cyclase domain, in agreement with the enzyme activity data. However, unlike the TRIR data for W104AzPhe $AppA_{BLUF}$ and W91AzPhe PixD, the AzPhe in OaPAC does not respond instantaneously to excitation, consistent with a Trp_{out} conformation in the dark state of OaPAC in contrast to the Trp_{in} conformation for $AppA_{BLUF}$ and PixD. The subsequent evolution of W90AzPhe on slower timescales reflect the protein structural changes that lead to the light activated state of OaPAC in which the AzPhe now samples a different environment consistent with a Trp_{in} conformation.

We also studied the importance of hydrogen bonding interactions between Y125 and N256 across the OaPAC dimer interface. Previous studies had shown that Y125F was catalytically inactive,[101,106] and we also demonstrated that replacement of N256 with Ala, Gln or Asp resulted in loss of activity. We then modulated the pK_a of Y125 by replacing this residue with fluoro-Tyr analogues that vary the acidity of the Tyr hydroxyl group. While 3F-Y125 OaPAC had similar activity to wild-type OaPAC, neither the 3,5-F_2Y125 or 2,3,5F_3Y125 OaPAC variants had detectable activity in the dark and light state. One possible explanation for this result is that Y125 has to be protonated for signal transduction to occur and that in 3,5-F_2Y125 and 2,3,5-F_3Y125 OaPAC the Tyr is deprotonated. To test this hypothesis, we attempted to protonate the fluoro-Tyr residues by lowering the pH. However, control experiments with wild-type OaPAC indicated that the enzyme rapidly lost activity at pH values below 8. All the fluoro-Tyr and N256 variants retained the red shift in the FAD absorbance and recovered to the dark state at rates similar to that of wild-type OaPAC, indicating that light-induced changes in the chromophore binding pocket are decoupled from enzyme activation.

Chapter 4: Summary and Future Directions

Summary:

Many natural proteins contain chromophores that transmit the ultrafast light signal into a biological response. The events that follow photoexcitation are controlled by the chromophore environment. My dissertation investigates the light-activated mechanism and signaling transduction of a photoactivated adenylate cyclase from a cyanobacterium *Oscillatoria acuminata,* OaPAC, which is a blue-light utilizing FAD (BLUF) photoreceptor, where absorption of light by the FAD triggers structural changes that ultimately modulate the cyclic AMP production consequently affect the signaling pathways involving the secondary messenger cAMP. Our overarching goal is to precisely determine how the instantaneous light-induced change in electronic structure of the flavin leads to: 1) ultrafast alterations in the protein matrix that surrounds the chromophore, and 2) structural evolution on the μs-ms timescale that results in activation of the functional domain of the photoreceptor. Such information will drive the application and optimization of these light-activated proteins as novel optogenetic tools to control biological processes using light. We employed steady-state FTIR and time-resolved infrared spectroscopy combined with incorporation of unnatural amino acids (UAAs) to investigate the photochemistry and signaling transduction in OaPAC.

Chapter 1 discusses in detail the model system (proteins and chromophore), as well as the specific methods employed to monitor the primary events of the light-induced reaction and the signaling transductions upon photoexcitation. Chapters 2 goes into more detail on the work we accomplished for the characterization of the photoactivation mechanism of OaPAC using unnatural amino acid mutagenesis to modulate the physical properties of the conserved tyrosine. The TRIR

measurements were extended to the BLUF protein OaPAC that contains an adenylyl cyclase domain covalently attached to the blue light sensing domain. OaPAC BLUF protein is a good model system not only for studying photochemistry but also signaling transduction by monitoring the conversion of ATP to cAMP and PPi. We employed ultrafast infrared and transient absorption to characterize the light-driven reaction. The photoactivation mechanism of wild-type OaPAC involves a concerted proton electron transfer from the conserved Y6 to excited FAD*. This mechanism is different from the one observed in PixD, where the photoactivation mechanism involves a sequential proton-coupled electron transfer from Y8 to excited FAD*. The role of Y6 in the photocycle of OaPAC was probed via unnatural amino acid mutagenesis. Replacement of Y6 with n-FY analogues increases the acidity of the phenol hydroxyl group and reduces the rate of electron transfer. Altering the pKa and/or reduction potential had a profound impact on the light-state formation for 2,3-F2Y6, 3,5-F2Y6 and 2,3,5-F3Y6 where the photocycle was halted at FAD●-. Only 2,3-F2Y6 variants showed a red shift in the UV-Vis measurement, but in the TRIR no stable light state was detected. Using spectrophotometric assay that couples a PPi production to consumption of NADH, we measured the enzyme activity for the wild type OaPAC and the n-FY6 variants to interrogate the ability of F-Tyr OaPAC variants to convert ATP to cAMP and PPi. The enzymatic assay results revealed that only n-FY6 variants with pKa 7.8 or higher were able to convert ATP to cAMP and PPi while variants with lower pKa were unable to turn on the enzyme since the photocycle was halted at FAD●-.

Future Directions:

Mutagenesis in OaPAC to modulate its photochemistry

There are still questions that remain to be elucidated for photochemistry and the signaling transduction of BLUF proteins. We do not fully understand what drives the formation of radical intermediates that lead to the formation of the light state in some BLUF proteins but not in others. It is quite intriguing how the BLUF core among BLUF proteins has similar architecture and the same conserved residues- tyrosine and glutamine, however, the photoactivation mechanism varies among them. We had studied BLUF proteins such as $AppA_{BLUF}$ and BlsA that do not form metastable radical intermediate in the light-driven reaction, whereas wild-type PixD and wild-type OaPAC form flavin radicals as an intermediate species. A future direction will be to make mutations in OaPAC that could possibly change its photochemistry from flavin radicals to no radical intermediates. Gil et al. pointed out key differences in the flavin binding pocket of $AppA_{BLUF}$ and PixD that might explain the variation in the mechanism.[54] A common residue found in PixD and OaPAC is an arginine (R65) that makes a hydrogen bonding interaction with C2=O group of the flavin while in AppABLUF is histidine. Computational studies show that arginine found in PixD is important for the stabilization of the flavin radicals.[69] Would replacing the arginine in OaPAC abolish the radical intermediates while keeping its chemistry? Making the histidine mutant in OaPAC will lead to a better understanding of the photoactivation mechanism among BLUF proteins.

Bibliography:

(1) Losi, A., Gardner, K. H., & Möglich, A. (2018). Blue-light receptors for optogenetics. *Chemical reviews*, *118*(21), 10659-10709.

(2) Van Der Horst, M. A., & Hellingwerf, K. J. (2004). Photoreceptor proteins,"star actors of modern times": a review of the functional dynamics in the structure of representative members of six different photoreceptor families. *Accounts of chemical research*, *37*(1), 13-20.

(3) Shcherbakova, D. M., Shemetov, A. A., Kaberniuk, A. A., & Verkhusha, V. V. (2015). Natural photoreceptors as a source of fluorescent proteins, biosensors, and optogenetic tools. *Annual review of biochemistry*, *84*(1), 519-550.

(4) Royant, A., Nollert, P., Edman, K., Neutze, R., Landau, E. M., Pebay-Peyroula, E., & Navarro, J. (2001). X-ray structure of sensory rhodopsin II at 2.1-Å resolution. *Proceedings of the National Academy of Sciences*, *98*(18), 10131-10136.

(5) Nagano, S., Guan, K., Shenkutie, S. M., Feiler, C., Weiss, M., Kraskov, A., ... & Hughes, J. (2020). Structural insights into photoactivation and signalling in plant phytochromes. *Nature Plants*, *6*(5), 581-588.

(6) Perman, B., Srajer, V., Ren, Z., Teng, T. Y., Pradervand, C., Ursby, T., ... & Moffat, K. (1998). Energy transduction on the nanosecond time scale: early structural events in a xanthopsin photocycle. *Science*, *279*(5358), 1946-1950.

(7) Halavaty, A. S., & Moffat, K. (2007). N-and C-terminal flanking regions modulate light-induced signal transduction in the LOV2 domain of the blue light sensor phototropin 1 from Avena sativa. *Biochemistry*, *46*(49), 14001-14009.

(8) Li, J., & Kitagawa, T. (2011). Applications of vibrational spectroscopy in the study of flavin-based photoactive proteins. *Journal of Spectroscopy*, *25*(6), 261-269.

(9) Conrad, K. S., Manahan, C. C., & Crane, B. R. (2014). Photochemistry of flavoprotein light sensors. *Nature chemical biology*, *10*(10), 801-809.

(10) O'Banion, C. P., & Lawrence, D. S. (2018). Optogenetics: a primer for chemists. *ChemBioChem*, *19*(12), 1201-1216.

(11) Lukacs, A., Eker, A. P., Byrdin, M., Brettel, K., & Vos, M. H. (2008). Electron hopping through the 15 Å triple tryptophan molecular wire in DNA photolyase occurs within 30 ps. *Journal of the American Chemical Society*, *130*(44), 14394-14395.

(12) Jorns, M. S.; Baldwin, E. T.; Sancar, G. B.; Sancar, A., Action Mechanism of Escherichia-Coli DNA Photolyase .2. Role of the Chromophores in Catalysis. J Biol Chem 1987, 262 (1), 486-491.

(13) Losi, A. (2007). Flavin-based blue-light photosensors: a photobiophysics update. *Photochemistry and photobiology*, *83*(6), 1283-1300.

(14) Lukacs, A., Brust, R., Haigney, A., Laptenok, S. P., Addison, K., Gil, A., ... & Meech, S. R. (2014). BLUF domain function does not require a metastable radical intermediate state. *Journal of the American Chemical Society*, *136*(12), 4605-4615.

(15) Yee, E. F., Chandrasekaran, S., Lin, C., & Crane, B. R. (2019). Physical methods for studying flavoprotein photoreceptors. In *Methods in enzymology* (Vol. 620, pp. 509-544). Academic Press.

(16) Ohki, M., Sugiyama, K., Kawai, F., Tanaka, H., Nihei, Y., Unzai, S., ... & Park, S. Y. (2016). Structural insight into photoactivation of an adenylate cyclase from a photosynthetic cyanobacterium. *Proceedings of the National Academy of Sciences*, *113*(24), 6659-6664.

(17) Gauden, M., Yeremenko, S., Laan, W., van Stokkum, I. H., Ihalainen, J. A., van Grondelle, R., ... & Kennis, J. T. (2005). Photocycle of the flavin-binding photoreceptor AppA, a bacterial transcriptional antirepressor of photosynthesis genes. *Biochemistry*, *44*(10), 3653-3662.

(18) Masuda, Shinji. "Light detection and signal transduction in the BLUF photoreceptors." *Plant and Cell Physiology* 54.2 (2013): 171-179.

(19) McDonough, K. A., & Rodriguez, A. (2012). The myriad roles of cyclic AMP in microbial pathogens: from signal to sword. *Nature Reviews Microbiology*, *10*(1), 27-38.

(20) Nagase, M., Nagashima, T., Hamada, S., Morishima, M., Tohyama, S., Arima-Yoshida, F., ... & Watabe, A. M. (2024). All-optical presynaptic plasticity induction by photoactivated adenylyl cyclase targeted to axon terminals. *Cell Reports Methods*, *4*(4).

(21) Linder, J. U., & Schultz, J. E. (2003). The class III adenylyl cyclases: multi-purpose signalling modules. *Cellular signalling*, *15*(12), 1081-1089.

(22) Hahn, D. K., Tusell, J. R., Sprang, S. R., & Chu, X. (2015). Catalytic mechanism of mammalian adenylyl cyclase: a computational investigation. *Biochemistry*, *54*(40), 6252-6262.

(23) Liu, Y., Ruoho, A. E., Rao, V. D., & Hurley, J. H. (1997). Catalytic mechanism of the adenylyl and guanylyl cyclases: modeling and mutational analysis. *Proceedings of the National Academy of Sciences*, *94*(25), 13414-13419.

(24) Bassler, J., Schultz, J. E., & Lupas, A. N. (2018). Adenylate cyclases: Receivers, transducers, and generators of signals. *Cellular signalling*, *46*, 135-144.

(25) Chretien, A., Nagel, M. F., Botha, S., de Wijn, R., Brings, L., Dörner, K., ... & Schubert, R. (2024). Light-induced Trpin/Metout switching during BLUF domain

activation in ATP-bound photoactivatable adenylate cyclase OaPAC. *Journal of Molecular Biology*, *436*(5), 168439.

(26) Stüven, Birthe, et al. "Characterization and engineering of photoactivated adenylyl cyclases." *Biological Chemistry* 400.3 (2019): 429-441.

(27) Ito, S.; Murakami, A.; Iseki, M.; Takahashi, T.; Higashi, S.; Watanabe, M. (2010) Differentiation of photocycle characteristics of flavin-binding BLUF domains of alpha- and beta-subunits of photoactivated adenylyl cyclase of Euglena gracilis *Photochem Photobiol Sci*, **9**, 1327-1335. DOI: 10.1039/c0pp00130a

(28) Iseki, M.; Matsunaga, S.; Murakami, A.; Ohno, K.; Shiga, K.; Yoshida, K.; Sugai, M.; Takahashi, T.; Hori, T.; Watanabe, M. (2002) A blue-light-activated adenylyl cyclase mediates photoavoidance in Euglena gracilis *Nature*, **415**, 1047-1051. DOI: 10.1038/4151047a

(29) Stierl, M.; Penzkofer, A.; Kennis, J. T.; Hegemann, P.; Mathes, T. (2014) Key residues for the light regulation of the blue light-activated adenylyl cyclase from Beggiatoa sp *Biochemistry*, **53**, 5121-5130. DOI: 10.1021/bi500479v

(30) Stierl, M.; Stumpf, P.; Udwari, D.; Gueta, R.; Hagedorn, R.; Losi, A.; Gartner, W.; Petereit, L.; Efetova, M.; Schwarzel, M.; Oertner, T. G.; Nagel, G.; Hegemann, P. (2011) Light modulation of cellular cAMP by a small bacterial photoactivated adenylyl cyclase, bPAC, of the soil bacterium Beggiatoa *J Biol Chem*, **286**, 1181-1188. DOI: 10.1074/jbc.M110.185496

(31) Nagahama, T.; Suzuki, T.; Yoshikawa, S.; Iseki, M. (2007) Functional transplant of photoactivated adenylyl cyclase (PAC) into Aplysia sensory neurons *Neurosci Res*, **59**, 81-88. DOI: 10.1016/j.neures.2007.05.015

(32) Jansen, V.; Alvarez, L.; Balbach, M.; Strunker, T.; Hegemann, P.; Kaupp, U. B.; Wachten, D. (2015) Controlling fertilization and cAMP signaling in sperm by optogenetics *Elife*, **4**. DOI: 10.7554/eLife.05161

(33) Losi, A. In *Flavins: Photochemistry and Photobiology*; The Royal Society of Chemistry: 2006; Vol. 6, p 217-269.

(34) Losi, A.; Gartner, W. (2011) Old chromophores, new photoactivation paradigms, trendy applications: flavins in blue light-sensing photoreceptors *Photochem Photobiol*, **87**, 491-510. DOI: 10.1111/j.1751-1097.2011.00913.x

(35) Masuda, S.; Bauer, C. E. (2002) AppA is a blue light photoreceptor that antirepresses photosynthesis gene expression in Rhodobacter sphaeroides *Cell*, **110**, 613-623. DOI: 10.1016/S0092-8674(02)00876-0

(36) Gauden, M.; Yeremenko, S.; Laan, W.; van Stokkum, I. H.; Ihalainen, J. A.; van Grondelle, R.; Hellingwerf, K. J.; Kennis, J. T. (2005) Photocycle of the flavin-binding

photoreceptor AppA, a bacterial transcriptional antirepressor of photosynthesis genes *Biochemistry*, **44**, 3653-3662. DOI: 10.1021/bi047359a

(37) Anderson, S.; Dragnea, V.; Masuda, S.; Ybe, J.; Moffat, K.; Bauer, C. (2005) Structure of a novel photoreceptor, the BLUF domain of AppA from Rhodobacter sphaeroides *Biochemistry*, **44**, 7998-8005. DOI: 10.1021/bi0502691

(38) Gauden, M.; van Stokkum, I. H. M.; Key, J. M.; Luhrs, D. C.; Van Grondelle, R.; Hegemann, P.; Kennis, J. T. M. (2006) Hydrogen-bond switching through a radical pair mechanism in a flavin-binding photoreceptor *Proc Natl Acad Sci U S A*, **103**, 10895-10900. DOI: 10.1073/pnas.0600720103

(39) Stelling, A. L.; Ronayne, K. L.; Nappa, J.; Tonge, P. J.; Meech, S. R. (2007) Ultrafast structural dynamics in BLUF domains: transient infrared spectroscopy of AppA and its mutants *J Am Chem Soc*, **129**, 15556-15564. DOI: 10.1021/ja074074n

(40) Lukacs, A.; Haigney, A.; Brust, R.; Zhao, R. K.; Stelling, A. L.; Clark, I. P.; Towrie, M.; Greetham, G. M.; Meech, S. R.; Tonge, P. J. (2011) Photoexcitation of the blue light using FAD photoreceptor AppA results in ultrafast changes to the protein matrix *J Am Chem Soc*, **133**, 16893-16900. DOI: 10.1021/ja2060098

(41) Iwata, T.; Nagai, T.; Ito, S.; Osoegawa, S.; Iseki, M.; Watanabe, M.; Unno, M.; Kitagawa, S.; Kandori, H. (2018) Hydrogen Bonding Environments in the Photocycle Process around the Flavin Chromophore of the AppA-BLUF domain *J Am Chem Soc*, **140**, 11982-11991. DOI: 10.1021/jacs.8b05123

(42) Domratcheva, T.; Grigorenko, B. L.; Schlichting, I.; Nemukhin, A. V. (2008) Molecular models predict light-induced glutamine tautomerization in BLUF photoreceptors *Biophys. J.*, **94**, 3872-3879. DOI: 10.1529/biophysj.107.124172

(43) Ohki, M.; Sato-Tomita, A.; Matsunaga, S.; Iseki, M.; Tame, J. R. H.; Shibayama, N.; Park, S. Y. (2017) Molecular mechanism of photoactivation of a light-regulated adenylate cyclase *Proc Natl Acad Sci U S A*, **114**, 8562-8567. DOI: 10.1073/pnas.1704391114

(44) Yuan, H.; Anderson, S.; Masuda, S.; Dragnea, V.; Moffat, K.; Bauer, C. (2006) Crystal structures of the Synechocystis photoreceptor Slr1694 reveal distinct structural states related to signaling *Biochemistry*, **45**, 12687-12694. DOI: 10.1021/bi061435n

(45) Chitrakar, I.; Iuliano, J. N.; He, Y.; Woroniecka, H. A.; Tolentino Collado, J.; Wint, J. M.; Walker, S. G.; Tonge, P. J.; French, J. B. (2020) Structural Basis for the Regulation of Biofilm Formation and Iron Uptake in A. baumannii by the Blue-Light-Using Photoreceptor, BlsA *ACS Infect Dis*, **6**, 2592-2603. DOI: 10.1021/acsinfecdis.0c00156

(46) Hall, C. R.; Tolentino Collado, J.; Iuliano, J. N.; Gil, A. A.; Adamczyk, K.; Lukacs, A.; Greetham, G. M.; Sazanovich, I.; Tonge, P. J.; Meech, S. R. (2019) Site-Specific Protein Dynamics Probed by Ultrafast Infrared Spectroscopy of a Noncanonical Amino Acid *J Phys Chem B*, **123**, 9592-9597. DOI: 10.1021/acs.jpcb.9b09425

(47) Brust, R.; Lukacs, A.; Haigney, A.; Addison, K.; Gil, A.; Towrie, M.; Clark, I. P.; Greetham, G. M.; Tonge, P. J.; Meech, S. R. (2013) Proteins in action: femtosecond to millisecond structural dynamics of a photoactive flavoprotein *J Am Chem Soc*, **135**, 16168-16174. DOI: 10.1021/ja407265p

(48) Brust, R.; Haigney, A.; Lukacs, A.; Gil, A.; Hossain, S.; Addison, K.; Lai, C. T.; Towrie, M.; Greetham, G. M.; Clark, I. P.; Illarionov, B.; Bacher, A.; Kim, R. R.; Fischer, M.; Simmerling, C.; Meech, S. R.; Tonge, P. J. (2014) Ultrafast Structural Dynamics of BlsA, a Photoreceptor from the Pathogenic Bacterium Acinetobacter baumannii *J Phys Chem Lett*, **5**, 220-224. DOI: 10.1021/jz4023738

(49) Hasegawa, K.; Masuda, S.; Ono, T. A. (2006) Light induced structural changes of a full-length protein and its BLUF domain in YcgF(Blrp), a blue-light sensing protein that uses FAD (BLUF) *Biochemistry*, **45**, 3785-3793. DOI: 10.1021/bi051820x

(50) Hirano, M.; Takebe, M.; Ishido, T.; Ide, T.; Matsunaga, S. (2019) The C-terminal region affects the activity of photoactivated adenylyl cyclase from Oscillatoria acuminata *Sci Rep*, **9**, 20262. DOI: 10.1038/s41598-019-56721-3

(51) Lukacs, A.; Brust, R.; Haigney, A.; Laptenok, S. P.; Addison, K.; Gil, A.; Towrie, M.; Greetham, G. M.; Tonge, P. J.; Meech, S. R. (2014) BLUF domain function does not require a metastable radical intermediate state *J Am Chem Soc*, **136**, 4605-4615. DOI: 10.1021/ja4121082

(52) Bonetti, C.; Mathes, T.; van Stokkum, I. H. M.; Mullen, K. M.; Groot, M. L.; van Grondelle, R.; Hegemann, P.; Kennis, J. T. M. (2008) Hydrogen Bond Switching among Flavin and Amino Acid Side Chains in the BLUF Photoreceptor Observed by Ultrafast Infrared Spectroscopy *Biophys. J.*, **95**, 4790-4802. DOI: 10.1529/biophysj.108.139246

(53) Haigney, A.; Lukacs, A.; Zhao, R. K.; Stelling, A. L.; Brust, R.; Kim, R. R.; Kondo, M.; Clark, I.; Towrie, M.; Greetham, G. M.; Illarionov, B.; Bacher, A.; Romisch-Margl, W.; Fischer, M.; Meech, S. R.; Tonge, P. J. (2011) Ultrafast infrared spectroscopy of an isotope-labeled photoactivatable flavoprotein *Biochemistry*, **50**, 1321-1328. DOI: 10.1021/bi101589a

(54) Gil, A. A.; Laptenok, S. P.; Iuliano, J. N.; Lukacs, A.; Verma, A.; Hall, C. R.; Yoon, G. E.; Brust, R.; Greetham, G. M.; Towrie, M.; French, J. B.; Meech, S. R.; Tonge, P. J. (2017) Photoactivation of the BLUF Protein PixD Probed by the Site-Specific Incorporation of Fluorotyrosine Residues *J Am Chem Soc*, **139**, 14638-14648. DOI: 10.1021/jacs.7b07849

(55) Haigney, A.; Lukacs, A.; Brust, R.; Zhao, R. K.; Towrie, M.; Greetham, G. M.; Clark, I.; Illarionov, B.; Bacher, A.; Kim, R. R.; Fischer, M.; Meech, S. R.; Tonge, P. J. (2012) Vibrational assignment of the ultrafast infrared spectrum of the photoactivatable flavoprotein AppA *J Phys Chem B*, **116**, 10722-10729. DOI: 10.1021/jp305220m

(56) Hense, A.; Herman, E.; Oldemeyer, S.; Kottke, T. (2015) Proton transfer to flavin stabilizes the signaling state of the blue light receptor plant cryptochrome *J Biol Chem*, **290**, 1743-1751. DOI: 10.1074/jbc.M114.606327

(57) Lukacs, A.; Zhao, R. K.; Haigney, A.; Brust, R.; Greetham, G. M.; Towrie, M.; Tonge, P. J.; Meech, S. R. (2012) Excited state structure and dynamics of the neutral and anionic flavin radical revealed by ultrafast transient mid-IR to visible spectroscopy *J Phys Chem B*, **116**, 5810-5818. DOI: 10.1021/jp2116559

(58) Pirisi, K.; Nag, L.; Fekete, Z.; Iuliano, J. N.; Tolentino Collado, J.; Clark, I. P.; Pecsi, I.; Sournia, P.; Liebl, U.; Greetham, G. M.; Tonge, P. J.; Meech, S. R.; Vos, M. H.; Lukacs, A. (2021) Identification of the vibrational marker of tyrosine cation radical using ultrafast transient infrared spectroscopy of flavoprotein systems *Photochem Photobiol Sci*, **20**, 369-378. DOI: 10.1007/s43630-021-00024-y

(59) Tokonami, S.; Onose, M.; Nakasone, Y.; Terazima, M. (2022) Slow Conformational Changes of Blue Light Sensor BLUF Proteins in Milliseconds *J Am Chem Soc*, **144**, 4080-4090. DOI: 10.1021/jacs.1c13121

(60) Immeln, D.; Weigel, A.; Kottke, T.; Perez Lustres, J. L. (2012) Primary events in the blue light sensor plant cryptochrome: intraprotein electron and proton transfer revealed by femtosecond spectroscopy *J Am Chem Soc*, **134**, 12536-12546. DOI: 10.1021/ja302121z

(61) Müller, P.; Bouly, J.-P.; Hitomi, K.; Balland, V.; Getzoff, E. D.; Ritz, T.; Brettel, K. (2014) ATP Binding Turns Plant Cryptochrome Into an Efficient Natural Photoswitch *Sci Rep*, **4**, 5175. DOI: 10.1038/srep05175

(62) Mathes, T.; van Stokkum, I. H. M.; Kennis, J. T. M. In *Methods Mol Biol* 2014; Vol. 1146, p 401-442.

(63) Gauden, M.; Grinstead, J. S.; Laan, W.; van Stokkum, I. H.; Avila-Perez, M.; Toh, K. C.; Boelens, R.; Kaptein, R.; van Grondelle, R.; Hellingwerf, K. J.; Kennis, J. T. (2007) On the role of aromatic side chains in the photoactivation of BLUF domains *Biochemistry*, **46**, 7405-7415. DOI: 10.1021/bi7006433

(64) Ishikita, H. (2008) Light-induced hydrogen bonding pattern and driving force of electron transfer in AppA BLUF domain photoreceptor *J Biol Chem*, **283**, 30618-30623. DOI: 10.1074/jbc.M803864200

(65) Tommos, C.; Babcock, G. T. (2000) Proton and hydrogen currents in photosynthetic water oxidation *Biochim Biophys Acta*, **1458**, 199-219. DOI: 10.1016/s0005-2728(00)00069-4

(66) Swinehart, W.; Deutsch, C.; Sarachan, K. L.; Luthra, A.; Bacusmo, J. M.; de Crecy-Lagard, V.; Swairjo, M. A.; Agris, P. F.; Iwata-Reuyl, D. (2020) Specificity in the biosynthesis of the universal tRNA nucleoside N (6)-threonylcarbamoyl adenosine (t(6)A)-TsaD is the gatekeeper *RNA*, **26**, 1094-1103. DOI: 10.1261/rna.075747.120

(67) O'Brien, W. E. (1976) A continuous spectrophotometric assay for argininosuccinate synthetase based on pyrophosphate formation *Anal Biochem*, **76**, 423-430. DOI: 10.1016/0003-2697(76)90337-7

(68) Gil, A. A.; Haigney, A.; Laptenok, S. P.; Brust, R.; Lukacs, A.; Iuliano, J. N.; Jeng, J.; Melief, E. H.; Zhao, R. K.; Yoon, E.; Clark, I. P.; Towrie, M.; Greetham, G. M.; Ng, A.; Truglio, J. J.; French, J. B.; Meech, S. R.; Tonge, P. J. (2016) Mechanism of the AppABLUF Photocycle Probed by Site-Specific Incorporation of Fluorotyrosine Residues: Effect of the Y21 pKa on the Forward and Reverse Ground-State Reactions *J Am Chem Soc*, **138**, 926-935. DOI: 10.1021/jacs.5b11115

(69) Goings, J. J.; Reinhardt, C. R.; Hammes-Schiffer, S. (2018) Propensity for Proton Relay and Electrostatic Impact of Protein Reorganization in Slr1694 BLUF Photoreceptor *J Am Chem Soc*, **140**, 15241-15251. DOI: 10.1021/jacs.8b07456

(70) Goyal, P.; Hammes-Schiffer, S. (2017) Role of active site conformational changes in photocycle activation of the AppA BLUF photoreceptor *Proc Natl Acad Sci U S A*, **114**, 1480-1485. DOI: 10.1073/pnas.1621393114

(71) Fujisawa, T.; Takeuchi, S.; Masuda, S.; Tahara, T. (2014) Signaling-State Formation Mechanism of a BLUF Protein PapB from the Purple Bacterium Rhodopseudomonas palustris Studied by Femtosecond Time-Resolved Absorption Spectroscopy *J Phys Chem B*, **118**, 14761-14773. DOI: 10.1021/jp5076252

(72) Zirak, P.; Penzkofer, A.; Schiereis, T.; Hegemann, P.; Jung, A.; Schlichting, I. (2006) Photodynamics of the small BLUF protein BlrB from Rhodobacter sphaeroides *J Photochem Photobiol B*, **83**, 180-194. DOI: 10.1016/j.jphotobiol.2005.12.015

(73) Kang, X. W.; Chen, Z.; Zhou, Z.; Zhou, Y.; Tang, S.; Zhang, Y.; Zhang, T.; Ding, B.; Zhong, D. (2021) Direct Observation of Ultrafast Proton Rocking in the BLUF Domain *Angew Chem Int Ed Engl*, e202114423. DOI: 10.1002/anie.202114423

(74) Deisseroth, K. Optogenetics *Nature Methods*, **2010**, *8*, 26-29. DOI: 10.1038/nmeth.f.324

(75) Moglich, A.; Moffat, K. Engineered photoreceptors as novel optogenetic tools *Photochem Photobiol Sci*, **2010**, *9*, 1286-1300. DOI: 10.1039/c0pp00167h

(76) Lindner, F.; Diepold, A. Optogenetics in bacteria - applications and opportunities *FEMS Microbiol Rev*, **2022**, *46*. DOI: 10.1093/femsre/fuab055

(77) Iuliano, J. N.; Collado, J. T.; Gil, A. A.; Ravindran, P. T.; Lukacs, A.; Shin, S.; Woroniecka, H. A.; Adamczyk, K.; Aramini, J. M.; Edupuganti, U. R.; Hall, C. R.; Greetham, G. M.; Sazanovich, I. V.; Clark, I. P.; Daryaee, T.; Toettcher, J. E.; French, J. B.; Gardner, K. H.; Simmerling, C. L.; Meech, S. R.; Tonge, P. J. Unraveling the Mechanism of a LOV Domain Optogenetic Sensor: A Glutamine Lever Induces Unfolding of the Jalpha Helix *ACS Chem Biol*, **2020**, *15*, 2752-2765. DOI: 10.1021/acschembio.0c00543

(78) Lukacs, A.; Tonge, P. J.; Meech, S. R. Photophysics of the Blue Light Using Flavin Domain *Acc Chem Res*, **2022**, *55*, 402-414. DOI: 10.1021/acs.accounts.1c00659

(79) Gomelsky, M.; Klug, G. BLUF: a novel FAD-binding domain involved in sensory transduction in microorganisms *Trends Biochem Sci*, **2002**, *27*, 497-500. DOI: 10.1016/S0968-0004(02)02181-3

(80) Masuda, S.; Bauer, C. E. AppA is a blue light photoreceptor that antirepresses photosynthesis gene expression in Rhodobacter sphaeroides *Cell*, **2002**, *110*, 613-623. DOI: 10.1016/S0092-8674(02)00876-0

(81) Okajima, K.; Yoshihara, S.; Fukushima, Y.; Geng, X.; Katayama, M.; Higashi, S.; Watanabe, M.; Sato, S.; Tabata, S.; Shibata, Y.; Itoh, S.; Ikeuchi, M. Biochemical and functional characterization of BLUF-type flavin-binding proteins of two species of cyanobacteria *J Biochem*, **2005**, *137*, 741-750. DOI: 10.1093/jb/mvi089

(82) Tuttobene, M. R.; Cribb, P.; Mussi, M. A. BlsA integrates light and temperature signals into iron metabolism through Fur in the human pathogen Acinetobacter baumannii *Sci Rep*, **2018**, *8*, 7728. DOI: 10.1038/s41598-018-26127-8

(83) Iseki, M.; Matsunaga, S.; Murakami, A.; Ohno, K.; Shiga, K.; Yoshida, K.; Sugai, M.; Takahashi, T.; Hori, T.; Watanabe, M. A blue-light-activated adenylyl cyclase mediates photoavoidance in Euglena gracilis *Nature*, **2002**, *415*, 1047-1051. DOI: 10.1038/4151047a

(84) Stierl, M.; Stumpf, P.; Udwari, D.; Gueta, R.; Hagedorn, R.; Losi, A.; Gartner, W.; Petereit, L.; Efetova, M.; Schwarzel, M.; Oertner, T. G.; Nagel, G.; Hegemann, P. Light modulation of cellular cAMP by a small bacterial photoactivated adenylyl cyclase, bPAC, of the soil bacterium Beggiatoa *J Biol Chem*, **2011**, *286*, 1181-1188. DOI: 10.1074/jbc.M110.185496

(85) Ohki, M.; Sugiyama, K.; Kawai, F.; Tanaka, H.; Nihei, Y.; Unzai, S.; Takebe, M.; Matsunaga, S.; Adachi, S.; Shibayama, N.; Zhou, Z.; Koyama, R.; Ikegaya, Y.; Takahashi, T.; Tame, J. R.; Iseki, M.; Park, S. Y. Structural insight into photoactivation of an

adenylate cyclase from a photosynthetic cyanobacterium *Proc Natl Acad Sci U S A*, **2016**, *113*, 6659-6664. DOI: 10.1073/pnas.1517520113

(86) Anderson, S.; Dragnea, V.; Masuda, S.; Ybe, J.; Moffat, K.; Bauer, C. Structure of a novel photoreceptor, the BLUF domain of AppA from Rhodobacter sphaeroides *Biochemistry*, **2005**, *44*, 7998-8005. DOI: 10.1021/bi0502691

(87) Stelling, A. L.; Ronayne, K. L.; Nappa, J.; Tonge, P. J.; Meech, S. R. Ultrafast structural dynamics in BLUF domains: transient infrared spectroscopy of AppA and its mutants *J Am Chem Soc*, **2007**, *129*, 15556-15564. DOI: 10.1021/ja074074n

(88) Masuda, S.; Hasegawa, K.; Ishii, A.; Ono, T. A. Light-induced structural changes in a putative blue-light receptor with a novel FAD binding fold sensor of blue-light using FAD (BLUF); Slr1694 of synechocystis sp. PCC6803 *Biochemistry*, **2004**, *43*, 5304-5313. DOI: 10.1021/bi049836v

(89) Gauden, M.; Yeremenko, S.; Laan, W.; van Stokkum, I. H.; Ihalainen, J. A.; van Grondelle, R.; Hellingwerf, K. J.; Kennis, J. T. Photocycle of the flavin-binding photoreceptor AppA, a bacterial transcriptional antirepressor of photosynthesis genes *Biochemistry*, **2005**, *44*, 3653-3662. DOI: 10.1021/bi047359a

(90) Unno, M.; Masuda, S.; Ono, T. A.; Yamauchi, S. Orientation of a key glutamine residue in the BLUF domain from AppA revealed by mutagenesis, spectroscopy, and quantum chemical calculations *J Am Chem Soc*, **2006**, *128*, 5638-5639. DOI: 10.1021/ja060633z

(91) Jung, A.; Reinstein, J.; Domratcheva, T.; Shoeman, R. L.; Schlichting, I. Crystal structures of the AppA BLUF domain photoreceptor provide insights into blue light-mediated signal transduction *J. Mol. Biol.*, **2006**, *362*, 717-732. DOI:

(92) Chretien, A.; Nagel, M. F.; Botha, S.; de Wijn, R.; Brings, L.; Dorner, K.; Han, H.; Koliyadu, J. C. P.; Letrun, R.; Round, A.; Sato, T.; Schmidt, C.; Secareanu, R. C.; von Stetten, D.; Vakili, M.; Wrona, A.; Bean, R.; Mancuso, A.; Schulz, J.; Pearson, A. R.; Kottke, T.; Lorenzen, K.; Schubert, R. Light-induced Trp(in)/Met(out) Switching During BLUF Domain Activation in ATP-bound Photoactivatable Adenylate Cyclase OaPAC *J Mol Biol*, **2024**, *436*, 168439. DOI: 10.1016/j.jmb.2024.168439

(93) PyMOL. The PyMOL Molecular Graphics System, Version 2.5 Schrödinger, LLC, **2015**. DOI:

(94) Lukacs, A.; Haigney, A.; Brust, R.; Zhao, R. K.; Stelling, A. L.; Clark, I. P.; Towrie, M.; Greetham, G. M.; Meech, S. R.; Tonge, P. J. Photoexcitation of the blue light using FAD photoreceptor AppA results in ultrafast changes to the protein matrix *J Am Chem Soc*, **2011**, *133*, 16893-16900. DOI: 10.1021/ja2060098

(95) Unno, M.; Kikuchi, S.; Masuda, S. Structural refinement of a key tryptophan residue in the BLUF photoreceptor AppA by ultraviolet resonance Raman spectroscopy *Biophys J*, **2010**, *98*, 1949-1956. DOI: 10.1016/j.bpj.2010.01.007

(96) Pandey, R.; Flockerzi, D.; Hauser, M. J.; Straube, R. Modeling the light- and redox-dependent interaction of PpsR/AppA in Rhodobacter sphaeroides *Biophys J*, **2011**, *100*, 2347-2355. DOI: 10.1016/j.bpj.2011.04.017

(97) Dragnea, V.; Arunkumar, A. I.; Lee, C. W.; Giedroc, D. P.; Bauer, C. E. A Q63E Rhodobacter sphaeroides AppA BLUF domain mutant is locked in a pseudo-light-excited signaling state *Biochemistry*, **2010**, *49*, 10682-10690. DOI: 10.1021/bi1002162

(98) Tolentino Collado, J.; Iuliano, J. N.; Pirisi, K.; Jewlikar, S.; Adamczyk, K.; Greetham, G. M.; Towrie, M.; Tame, J. R. H.; Meech, S. R.; Tonge, P. J.; Lukacs, A. Unraveling the Photoactivation Mechanism of a Light-Activated Adenylyl Cyclase Using Ultrafast Spectroscopy Coupled with Unnatural Amino Acid Mutagenesis *ACS Chem Biol*, **2022**, *17*, 2643-2654. DOI: 10.1021/acschembio.2c00575

(99) Tolentino Collado, J.; Bodis, E.; Pasitka, J.; Szucs, M.; Fekete, Z.; Kis-Bicskei, N.; Telek, E.; Pozsonyi, K.; Kapetanaki, S. M.; Greetham, G.; Tonge, P. J.; Meech, S. R.; Lukacs, A. Single Amino Acid Mutation Decouples Photochemistry of the BLUF Domain from the Enzymatic Function of OaPAC and Drives the Enzyme to a Switched-on State *J Mol Biol*, **2024**, *436*, 168312. DOI: 10.1016/j.jmb.2023.168312

(100) Raics, K.; Pirisi, K.; Zhuang, B.; Fekete, Z.; Kis-Bicskei, N.; Pecsi, I.; Ujfalusi, K. P.; Telek, E.; Li, Y.; Collado, J. T.; Tonge, P. J.; Meech, S. R.; Vos, M. H.; Bodis, E.; Lukacs, A. Photocycle alteration and increased enzymatic activity in genetically modified photoactivated adenylate cyclase OaPAC *J Biol Chem*, **2023**, *299*, 105056. DOI: 10.1016/j.jbc.2023.105056

(101) Ohki, M.; Sato-Tomita, A.; Matsunaga, S.; Iseki, M.; Tame, J. R. H.; Shibayama, N.; Park, S. Y. Molecular mechanism of photoactivation of a light-regulated adenylate cyclase *Proc Natl Acad Sci U S A*, **2017**, *114*, 8562-8567. DOI: 10.1073/pnas.1704391114

(102) Hall, C. R.; Tolentino Collado, J.; Iuliano, J. N.; Gil, A. A.; Adamczyk, K.; Lukacs, A.; Greetham, G. M.; Sazanovich, I.; Tonge, P. J.; Meech, S. R. Site-Specific Protein Dynamics Probed by Ultrafast Infrared Spectroscopy of a Noncanonical Amino Acid *J Phys Chem B*, **2019**, *123*, 9592-9597. DOI: 10.1021/acs.jpcb.9b09425

(103) Krause, B. S.; Kaufmann, J. C. D.; Kuhne, J.; Vierock, J.; Huber, T.; Sakmar, T. P.; Gerwert, K.; Bartl, F. J.; Hegemann, P. Tracking Pore Hydration in Channelrhodopsin by Site-Directed Infrared-Active Azido Probes *Biochemistry*, **2019**, *58*, 1275-1286. DOI: 10.1021/acs.biochem.8b01211

(104) Kurttila, M.; Stucki-Buchli, B.; Rumfeldt, J.; Schroeder, L.; Hakkanen, H.; Liukkonen, A.; Takala, H.; Kottke, T.; Ihalainen, J. A. Site-by-site tracking of signal transduction in an azidophenylalanine-labeled bacteriophytochrome with step-scan FTIR spectroscopy *Phys Chem Chem Phys*, **2021**, *23*, 5615-5628. DOI: 10.1039/d0cp06553f

(105) Noren, C. J.; Anthony-Cahill, S. J.; Griffith, M. C.; Schultz, P. G. A general method for site-specific incorporation of unnatural amino acids into proteins *Science*, **1989**, *244*, 182-188. DOI: 10.1126/science.2649980

(106) Lindner, R.; Hartmann, E.; Tarnawski, M.; Winkler, A.; Frey, D.; Reinstein, J.; Meinhart, A.; Schlichting, I. Photoactivation Mechanism of a Bacterial Light-Regulated Adenylyl Cyclase *J Mol Biol*, **2017**, *429*, 1336-1351. DOI: 10.1016/j.jmb.2017.03.020

(107) Yuan, H.; Anderson, S.; Masuda, S.; Dragnea, V.; Moffat, K.; Bauer, C. Crystal structures of the Synechocystis photoreceptor Slr1694 reveal distinct structural states related to signaling *Biochemistry*, **2006**, *45*, 12687-12694. DOI: 10.1021/bi061435n

(108) Masuda, S.; Tomida, Y.; Ohta, H.; Takamiya, K. The critical role of a hydrogen bond between Gln63 and Trp104 in the blue-light sensing BLUF domain that controls AppA activity *J Mol Biol*, **2007**, *368*, 1223-1230. DOI: 10.1016/j.jmb.2007.02.087

(109) Brust, R.; Lukacs, A.; Haigney, A.; Addison, K.; Gil, A.; Towrie, M.; Clark, I. P.; Greetham, G. M.; Tonge, P. J.; Meech, S. R. Proteins in action: femtosecond to millisecond structural dynamics of a photoactive flavoprotein *J Am Chem Soc*, **2013**, *135*, 16168-16174. DOI: 10.1021/ja407265p

(110) Tokonami, S.; Onose, M.; Nakasone, Y.; Terazima, M. Slow Conformational Changes of Blue Light Sensor BLUF Proteins in Milliseconds *J Am Chem Soc*, **2022**, *144*, 4080-4090. DOI: 10.1021/jacs.1c13121

(111) Goyal, P.; Hammes-Schiffer, S. Role of active site conformational changes in photocycle activation of the AppA BLUF photoreceptor *Proc Natl Acad Sci U S A*, **2017**, *114*, 1480-1485. DOI: 10.1073/pnas.1621393114

(112) Grinstead, J. S.; Hsu, S. T.; Laan, W.; Bonvin, A. M.; Hellingwerf, K. J.; Boelens, R.; Kaptein, R. The solution structure of the AppA BLUF domain: insight into the mechanism of light-induced signaling *Chembiochem*, **2006**, *7*, 187-193. DOI: 10.1002/cbic.200500270

(113) Zhou, Y.; Tang, S.; Chen, Z.; Zhou, Z.; Huang, J.; Kang, X. W.; Zou, S.; Wang, B.; Zhang, T.; Ding, B.; Zhong, D. Origin of the multi-phasic quenching dynamics in the BLUF domains across the species *Nat Commun*, **2024**, *15*, 623. DOI: 10.1038/s41467-023-44565-5

(114) Nakasone, Y.; Murakami, H.; Tokonami, S.; Oda, T.; Terazima, M. Time-resolved study on signaling pathway of photoactivated adenylate cyclase and its nonlinear optical response *J Biol Chem*, **2023**, *299*, 105285. DOI: 10.1016/j.jbc.2023.105285

(115) Seyedsayamdost, M. R.; Yee, C. S.; Stubbe, J. Site-specific incorporation of fluorotyrosines into the R2 subunit of E. coli ribonucleotide reductase by expressed protein ligation *Nat Protoc*, **2007**, *2*, 1225-1235. DOI: 10.1038/nprot.2007.159

(116) Seyedsayamdost, M. R.; Reece, S. Y.; Nocera, D. G.; Stubbe, J. Mono-, di-, tri-, and tetra-substituted fluorotyrosines: new probes for enzymes that use tyrosyl radicals in catalysis *J Am Chem Soc*, **2006**, *128*, 1569-1579. DOI: 10.1021/ja055926r

(117) Greetham, G. M.; Sole, D.; Clark, I. P.; Parker, A. W.; Pollard, M. R.; Towrie, M. Time-resolved multiple probe spectroscopy *Rev Sci Instrum*, **2012**, *83*, 103107. DOI: 10.1063/1.4758999

(118) Greetham, G. M.; Burgos, P.; Cao, Q.; Clark, I. P.; Codd, P. S.; Farrow, R. C.; George, M. W.; Kogimtzis, M.; Matousek, P.; Parker, A. W.; Pollard, M. R.; Robinson, D. A.; Xin, Z. J.; Towrie, M. ULTRA: A Unique Instrument for Time-Resolved Spectroscopy *Appl Spectrosc*, **2010**, *64*, 1311-1319. DOI: 10.1366/000370210793561673